SURE 静岡大学学術リポジトリ
Shizuoka University REpository

Rationally Designed Strigolactone Analogs as Antagonists of the D14 Receptor

メタデータ	言語: English 出版者: 公開日: 2019-01-16 キーワード (Ja): キーワード (En): antagonist, receptor, strigolactones 作成者: Takeuchi, Jun, Jiang, Kai, Hirabayashi, Kei, Imamura, Yusaku, Wu, Yashan, Xu, Yuqun, Miyakawa, Takuya, Nakamura, Hidemitsu, Tanokura, Masaru, Asami, Tadao メールアドレス: 所属:
URL	http://hdl.handle.net/10297/00026252

Rationally Designed Strigolactone Analogs as Antagonists of the D14 Receptor

Carba-SL compounds for inhibiting SL receptors

Corresponding Author:

Tadao Asami, PhD

Department of Applied Biological Chemistry

The University of Tokyo

1-1-1 Yayoi, Bunkyo-ku, Tokyo 113-8657, Japan

Tel/fax: +81 3 5841 5157

E-mail: asami@mail.ecc.u-tokyo.ac.jp

Subject Areas:

Proteins, enzymes and metabolism

Growth and development

Black and white figure: 5

Color figure: 3

Table: 0

Supplementary material: 12 (Fig. S1–S12)

Rationally Designed Strigolactone Analogs as Antagonists of the D14 Receptor

Carba-SL compounds for inhibiting SL receptors

Jun Takeuchi[1,a], Kai Jiang[2,a], Kei Hirabayashi[3,a], Yusaku Imamura[2], Yashan Wu[2], Yuqun Xu[3], Takuya Miyakawa[3], Hidemitsu Nakamura[2], Masaru Tanokura[3], Tadao Asami[2,4*]

[1]*Faculty of Agriculture, Shizuoka University, Shizuoka 422-8529, Japan*

[2]*Department of Applied Biological Chemistry, The University of Tokyo, Tokyo 113-8657, Japan*

[3]*Laboratory of Basic Science on Healthy Longevity, Department of Applied Biological Chemistry, The University of Tokyo, Tokyo 113-8657, Japan*

[4]*Department of Biochemistry, King Abdulaziz University, Jeddah 21589, Saudi Arabia*

[a]*These authors contributed equally to this work.*

*E-mail: asami@mail.ecc.u-tokyo.ac.jp

Abbreviations: AtD14, Arabidopsis DWARF14; 4BD, 4-bromo debranone; D3, dwarf3; D53, dwarf53; DAD2, decreased apical dominance 2; DIAD, diisopropyl azodicarboxylate; 4-DMAP, 4-(dimethylamino) pyridine; Et_3N, triethylamine; EtOAc, ethyl acetate; HTL, hyposensitive to light; KAI2, karrikin insensitive 2; MAX2, more axillary growth 2; NMP, N-methylpyrrolidone; NMR, nuclear magnetic resonance; PDB, protein data bank; Ph_3P, triphenylphosphine; RMS3, ramosus3; r.m.s.d., root mean square deviation; SL, strigolactone; SMXL, suppressor of more axillary growth2-like; THF, tetrahydrofuran; t_R, retention time; YLG, Yoshimulactone green.

Abstract

Strigolactones (SLs) are plant hormones that inhibit shoot branching and act as signals in communications with symbiotic fungi and parasitic weeds in the rhizosphere. SL signaling is mediated by DWARF14 (D14), which is an α/β-hydrolase that cleaves SLs into an ABC tricyclic lactone and a butenolide group (i.e., D-ring). This cleavage reaction (hydrolysis and dissociation) is important for inducing the interaction between D14 and its target proteins, including D3 and D53. In this study, a hydrolysis-resistant SL analog was predicted to inhibit the activation of the D14 receptor, thereby disrupting the SL signaling pathway. To test this prediction, carba-SL compounds, in which the ether oxygen of the D-ring or the phenol ether oxygen of the SL agonist (GR24 or 4-bromo debranone) was replaced with a methylene group, were synthesized as novel D14 antagonists. Subsequent biochemical and physiological studies indicated that carba-SLs blocked the interaction between D14 and D53 by inhibiting D14 hydrolytic activity. They also suppressed the SL-induced inhibition of rice tiller outgrowths. Additionally, carba-SLs antagonized the SL response in a *Striga* parasitic weed species. Structural analyses revealed that the D-ring of 7′-carba-4BD was hydrolyzed by D14 but did not dissociate from the 4BD skeleton. Thus, 7′-carba-4BD functioned as an antagonist rather than an agonist. Thus, the hydrolysis of the D-ring of SLs may be insufficient for activating the receptor. This study provides data relevant to designing SL receptor antagonists.

Keywords: antagonist, receptor, strigolactones

Introduction

Strigolactones (SLs) are plant hormones that regulate various physiological processes, such as shoot branching, root development and leaf senescence (Gomez-Roldan et al. 2008, Umehara et al. 2008, Brewer et al, 2013), and they play key roles in plant rhizospheric communication with symbiotic fungi and parasitic weeds (Xie et al. 2010, Akiyama et al. 2005). For example, root-derived SLs induce the hyphal branching of arbuscular mycorrhizal fungi and trigger the seed germination of parasitic weeds, including *Striga* and *Orobanche* species, which are severe threats to agricultural production in sub-Saharan Africa (Cook et al. 1966, Ejeta, 2007). Canonical SLs possess a four-ring structure, with a tricyclic lactone (ABC-ring) connected to a butenolide group (D-ring) *via* an enol ether bridge. The D-ring portion is present in all bioactive SLs, whereas the ABC-ring is chemically modified in many natural SLs (de Saint Germain et al. 2013).

The physiological actions of SLs are controlled by signal transduction involving the AtD14/D14/DAD2/RMS3 (*Arabidopsis thaliana*/rice/petunia/pea, respectively) receptors, which are members of the α/β-hydrolase superfamily that contain the Ser–His–Asp catalytic triad in a hydrophobic active site (Seto and Yamaguchi, 2014). By binding to AtD14, GR24, which is a synthetic SL analog, is hydrolyzed and converted to a D-ring-derived intermediate (covalently linked intermediate molecule) (de Saint Germain et al. 2016, Yao et al. 2016). This process initiates a conformational change in the receptor, which causes the ligand-binding pocket to close (Yao et al. 2016). The pocket is open in the apoenzyme state, but closes to create a surface that can bind to F-box proteins, including MAX2 in *A. thaliana* and D3 in rice. The AtD14-bound MAX2/D3 probably interacts with SMXLs (D53s in rice), which repress SL signaling, to induce their degradation through the proteasome-ubiquitin pathway, thereby enabling SL signal transduction to proceed (Jiang et al. 2013, Zhou et al. 2013, Wang et al. 2015, Waters et al. 2017). In this system, the conformational change in the key regulatory

protein, AtD14, is allosterically controlled by the cleavage of SLs. SL receptors in various plant species also cleave SLs, and the conformational destabilization of the receptor proteins affects SL signaling (Hamiaux et al. 2012, Nakamura et al. 2013, Zhao et al. 2015, de Saint Germain et al. 2016). However, the functional implication of the receptor-mediated SL hydrolysis and the active forms of SLs remain controversial (Carlsson et al. 2018).

A chemical compound that activates or inhibits SL signaling would be valuable for investigating SL functions in plant physiological processes, either independently or in combination with genetic methods. Additionally, an SL-signaling modulator would be of potential agrichemical value, because the ability to control shoot architecture and rhizosphere signals is important for effective and stable agricultural production (Nakamura and Asami, 2014). Although many SL receptor agonists, such as GR24 and 4-bromo debranone (4BD), have been previously described (Fukui et al. 2011, Lumba et al. 2017), there are currently only four reports describing the associated antagonists. Three of these antagonists, soporidine, 2-methoxy-1-naphthaldehyde and tolfenamic acid, were discovered by screening chemicals (Holbrook-smith et al. 2016, Mashita et al. 2016, Hamiaux et al. 2018). Additionally, the TFQ compounds were designed as covalent inhibitors of α/β-hydrolases (Xiang et al. 2017). Soporidine inhibits the *Striga* species' SL receptor (HTL7) and suppresses the germination of *Striga* species' seeds. 2-Methoxy-1-naphthaldehyde inhibits the GR24-induced interaction between D14 and D53 and restores the rice tiller outgrowth suppressed by GR24. Tolfenamic acid inhibits DAD2's catalytic activity and interferes with the GR24-induced inhibition of branch growth in petunia. The TFQ compounds, which have a β-propiolactone ring, irreversibly bind to the conserved serine residue of the catalytic triad and inhibit AtD14 and HTL7 activities. These compounds may represent chemical probes that could be useful for characterizing SL functions. However, we must consider their potential off-target effects *via* other α/β-hydrolases because they are structurally completely different from the SLs reported

to date. Therefore, in this study, we designed novel SL receptor antagonists, carba-SL compounds (**3**–**5**; Fig. 1), as structural analogs of GR24 and 4BD based on the structural requirement for SL bioactivity and the mechanism for activating the receptor. We describe the design, synthesis, and *in vitro* and *in vivo* activities of carba-SL compounds as antagonists capable of blocking SL signaling in rice and *Striga* species.

Results

Design and synthesis

The D14 protein includes a conserved catalytic triad, Ser-His-Asp, at the bottom of the ligand-binding pocket and hydrolytically cleaves the enol ether moiety between the C- and D-rings of SLs. Although the D-ring of SLs is essential for biological functions (Zwanenburg et al. 2013, Umehara et al. 2014), the activity of D-OH, a product of SL hydrolysis, is significantly lower than that of intact SLs, such as GR24 (Nakamura et al. 2013). These observations suggest that the hydrolysis reaction plays a key role in the activation of D14. Additionally, the crystal structure of the AtD14-D3 complex indicates that the serine residue of the catalytic triad attacks the carbonyl group of the SL D-ring to initiate hydrolysis. The resulting D-ring-derived intermediate is trapped in the catalytic active site, which triggers a conformational change in AtD14 (Yao et al. 2016). Therefore, hydrolysis-resistant SL analogs may function as D14 antagonists by competitively inhibiting the hydrolytic activity of D14.

Based on the above considerations, we designed the following novel D14 antagonists: (±)-1′-carba-GR24 (compound **3**) and (±)-1′-carba-4BD (compound **4**), in which the butenolide rings of GR24 and 4BD, respectively, are replaced with cyclopentenone rings, and (±)-7′-carba-4BD (compound **5**), in which the phenol ether oxygen of 4BD is replaced by a CH_2 group. These compounds should be incapable of reacting with the catalytic triad of D14. Accordingly, if they are accepted by the ligand-binding pocket, they would block SL

signaling. (±)-1′-Carba-GR24 and (±)-1′-carba-4BD were synthesized as shown in Fig. 2A and B, respectively. Compound **7** (West et al. 1993, Thuring et al. 1997a) was introduced to compound **6** using previously reported conditions (Mangnus et al. 1992) to generate (±)-1′-carba-GR24 (**3**), which was used as a diastereomeric mixture. 4-Bromophenol was introduced to compound **8** (Baraldi et al. 1986) *via* the Mitsunobu reaction to generate (±)-1′-carba-4BD (**4**). (±)-7′-Carba-4BD was synthesized as shown in Fig. 2C. Compound **9** (Eleftheriadis et al. 2016) was treated with vinylmagnesium bromide to yield alcohol **10** (Louvel et al. 2013). The introduction of a methacrylaldehyde by treating alcohol **10** with methacryloyl chloride in the presence of triethylamine and 4-(dimethylamino) pyridine yielded allylic ester **11** (Calad and Woerpel, 2007). The allylic ester **11** was then treated with 6 mol% second generation Grubbs catalyst to generate (±)-7′-carba-4BD (**5**). All (±)-carba-SL compounds (**3**–**5**) were obtained by organic synthesis.

Physiological effects of carba-SL compounds on rice tiller growth

The biological activities of carba-SL compounds were examined using the rice tillering assay, which is based on the inhibitory effects of SLs on tiller outgrowth. In hydroponically grown rice seedlings, the first and second tiller buds of SL-deficient mutants, including *d10* and *d17*, grow out, whereas those of wild-type plants remain dormant (Umehara et al. 2008). In the current study, D14 agonists suppressed tiller bud outgrowth, while D14 antagonists relieved this suppression when co-treated with D14 agonists, such as GR24, in SL-deficient mutants. None of the carba-SLs suppressed the tiller bud outgrowth of *d10-2* seedlings (Supplementary Fig S1). Additionally, the carba-SLs inhibited the GR24-induced suppression (Fig. 3A–C and Supplementary Fig. S2). These physiological data suggested that carba-SLs acted as antagonists of the rice SL receptor.

Biochemical characterization of carba-SL compounds

The stability of carba-SLs against D14 hydrolytic activity was examined using recombinant rice D14 produced in *Escherichia coli*. The stability of (±)-1′-carba-GR24 and (±)-7′-carba-4BD against hydrolysis was evaluated based on decreases in the amounts of substrates after an incubation with D14. There were no differences in the amounts of both compounds in the absence or presence of D14, whereas the amount of GR24 decreased significantly in the presence of D14 (Fig. 4A and Supplementary Fig. S3). In addition, the resistance of (±)-1′-carba-4BD to hydrolysis was monitored by measuring the amount of 4-bromophenol, which is the phenolic compound generated by D14 hydrolytic activity, because 4BD and (±)-1′-carba-4BD were degraded nonenzymatically under our assay conditions (Supplementary Fig. S4. We observed that 4BD was enzymatically converted to 4-bromophenol, and the amount of 4-bromophenol derived from (±)-1′-carba-4BD did not change in the presence of D14 (Fig. 4B and Supplementary Fig. S5). These results indicated that carba-SLs were not cleaved by D14, which was consistent with predictions based on the proposed model of AtD14-mediated hydrolysis of SLs.

Next, we examined the inhibitory effects of carba-SLs on D14 hydrolytic activity using fluorescence-based competition assays. In these assays, a profluorescent probe, Yoshimulactone Green (YLG) (Tsuchiya et al. 2015), was used as a substrate. SL receptors catalyze single-turnover reactions and form covalent bonds with the SL hydrolysate (Yao et al. 2016, de Saint Germain et al. 2016). Consequently, kinetic analyses are very complex. Therefore, we determined the inhibitor concentrations necessary to halve the response (IC_{50}) value for the formation of the fluorophore instead of the K_I value. All carba-SLs inhibited the D14-mediated YLG hydrolysis in a dose-dependent manner, and the IC_{50} values of (±)-1′-carba-GR24, (±)-1′-carba-4BD and (±)-7′-carba-4BD were 33.0 ± 0.6, 7.5 ± 1.8 and 17.8 ± 5.2 μM, respectively, when 0.3 μM YLG was used as the substrate (Fig. 5). These

values were higher than those of GR24 (1.5 ± 0.1 μM) and 4BD (3.2 ± 0.7 μM), suggesting that the affinities of carba-SLs for D14 are lower than those of SL agonists probably because carba-SLs do not form covalent bonds with the catalytic triad of D14. We also investigated the inhibitory activity levels of (±)-1′-carba-GR24 and (±)-1′-carba-4BD on the D14-catalyzed hydrolytic cleavage of GR24. The IC_{50} values of (±)-1′-carba-GR24 and (±)-1′-carba-4BD were 24.2 ± 4.0 and 16.6 ± 4.0 μM, respectively, when 10 μM GR24 was used as the substrate (Supplementary Fig. S6).

The effects of carba-SLs on the interaction between D14 and D53, which is a negative regulator of SL signaling, were examined using a yeast two-hybrid assay (Mashita et al. 2016). None of the carba-SLs induced the D14–D53 interaction, even at 50 μM, under our assay conditions (Fig. 6A). The antagonistic activities of these compounds were evaluated by examining their abilities to reverse the interaction between D14 and D53 induced by 1 μM GR24. All carba-SLs inhibited the interaction at 50 μM, although to varying degrees (Fig. 6B). The inhibitory activity of (±)-1′-carba-4BD was greater than that of (±)-1′-carba-GR24 or (±)-7′-carba-4BD, which was consistent with the results of the YLG competition assay. Thus, these biochemical data suggested that carba-SL compounds competitively inhibited the enzymatic activity of D14 and blocked the interaction between D14 and D53.

Structural analysis of the D14–7′-carba-4BD complex

To elucidate the molecular basis of the antagonism of carba-SLs toward D14, we analyzed the crystal structure of a D14–carba-SL complex. We examined only D14–7′-carba-4BD because we were unable to crystallize the D14–1′-carba-GR24 and D14–1′-carba-4BD complexes. The crystal structure of recombinant D14 bound to 7′-carba-4BD was determined at 1.90 Å resolution (Fig. 7A and Supplementary Table S1). The asymmetric unit contained two D14 molecules with almost identical structures. The r.m.s.d. was 0.34 Å for the main chain Cα atoms. As previously reported, D14 consists of a core domain, which is also known as the

α/β-hydrolase domain (Nardini and Dijkstra 1999), and a cap domain composed of four helices forming two antiparallel V shapes (Fig. 7A and Supplementary Fig. S7A). A catalytic pocket forms between the two domains. The catalytic residue, Ser147, is located at the bottom of the pocket and is aligned with His 297 and Asp268 to form the catalytic triad. The electron density map indicated that 7′-carba-4BD was present in the pocket (Fig. 7B). However, the D-ring of 7′-carba-4BD was unexpectedly observed in its open form (i.e., as a carboxylic acid) (Fig. 7B), and the electron density map was confirmed according to the method of Carlsson et al. (2018; Supplementary Fig. S8). These observations suggested that the butenolide ring of 7′-carba-4BD was hydrolyzed by the catalytic Ser147 in a manner similar to that of GR24 and 4BD.

In this complex structure, the hydrolyzed D-ring of 7′-carba-4BD faced the bottom of the catalytic pocket, while the bromo group partially protruded out of the pocket and was directly exposed to the solvent. This binding site consisted of Ser147, Val148, Val194, Val240, Cys241, Val244, Val269, Ser270 and several aromatic residues, including Phe78, Phe176, Phe186, Trp205, Tyr209, Phe245 and His297 (Supplementary Fig. S7B). These residues formed favorable hydrophobic and/or van der Waals interactions with the D-ring-opened 7′-carba-4BD. Additionally, the carboxyl group formed a strong hydrogen bond network with Phe78, Ser147, Tyr209 and His297 that was mediated by two water molecules (Fig. 7B). When the structure of this complex was superposed on that of the D14–GR24 complex (PDB code 5DJ5; Zhao LH. et al. 2015), no significant structural changes were observed in the enzyme, whereas the binding modes of each ligand were significantly different (Fig. 7C and Supplementary Fig. S7C). In the D14-D-ring-opened 7′-carba-4BD complex, the carboxyl group moved away from the catalytic triad because of the opening of the D-ring. This shift created space for the water molecules, mediating the hydrogen bond network. However, because 7′-carba-4BD did not generate a covalently linked intermediate molecule that induces

a conformational change in the receptor, the interaction between 7′-carba-4BD and D14 did not activate the receptor. Thus, 7′-carba-4BD acted as an antagonist rather than an agonist.

Effects of carba-SL compounds on a Striga parasitic weed species

Having established that carba-SLs function as antagonists of D14, we next tested their effects on a *Striga* parasitic weed species. When added to conditioned *Striga hermonthica* seeds imbibed with GR24, all of the carba-SLs decreased the germination rate in a dose-dependent manner, as expected for antagonists (Fig. 8A). *S. hermonthica* has a set of karrikin-receptor-like proteins (ShKAI2s/ShHTLs), including ShHTL7, which is exquisitely sensitive to natural SLs (Conn et al. 2015, Tsuchiya et al. 2015, Ehrhardt et al. 2015) and acts as both an enzyme and a receptor, like AtD14 (Yao et al. 2017). This suggests that ShHTL7 is the key receptor for the SL-dependent germination response of *S. hermonthica* seeds. Therefore, we examined the ability of carba-SLs to inhibit YLG hydrolysis using purified ShHTL7. The IC_{50} values of the compounds were less than 10 μM when 0.3 μM YLG was used as the substrate. This demonstrated that carba-SLs were able to inhibit ShHTL7's hydrolytic activity (Fig. 8B). Thus, the effects of carba-SLs appeared to not be restricted to the host rice plant.

Discussion

In this study, we synthesized novel SL receptor antagonists that were structural analogs of GR24 or 4BD. These carba-SL compounds were designed so that they were not hydrolyzed by their receptors. The structural, biological and physiological data presented here revealed that carba-SLs bound to the ligand-binding pocket of D14 and blocked the SL-induced interaction between D14 and D53 by inhibiting D14's hydrolytic activity. However, an analysis of the D14–7′-carba-4BD crystal structure indicated that the D-ring of 7′-carba-4BD was hydrolyzed by D14, which contradicted the results of the hydrolysis experiment. This

discrepancy may be the result of differences in the reaction times. Specifically, the D-ring of 7′-carba-4BD may be slowly hydrolyzed during protein crystallization, although we cannot exclude the possibility that the hydrolyzed D-ring re-cyclized into a butenolide ring during the extraction process of the hydrolysis assay. In either case, the D-ring of 7′-carba-4BD was hydrolyzed by D14 but did not dissociate from the 4BD skeleton. Consequently, 7′-carba-4BD acted as an antagonist rather than an agonist in all experiments. Thus, SL hydrolysis (i.e., opening of the D-ring) by D14 may be essential but not sufficient to activate the receptor. Thus, as with AtD14 and RMS3, the covalent bond that forms between the catalytic triad and the D-ring-derived SL hydrolysate may be important in inducing the interactions between D14 and its target proteins, including D53 and D3.

Before SLs were discovered as plant hormones, 7′-carba-GR24, in which the enol ether oxygen is replaced by a methylene group, was synthesized as a candidate compound for inhibiting the germination of parasitic weed seeds. At that time, the enol ether part was predicted to be a nucleophile attack site in the SL receptor. However, 7′-carba-GR24 did not inhibit the GR24-induced germination of *S. hermonthica* seeds (Thuring et al., 1997b). Additionally, recent studies indicated that 7′-carba-GR24 could neither induce nor inhibit the interaction between AtD14 and MAX2 (Yao et al. 2016, Xiang et al. 2017). However, our results revealed that 1′-carba-GR24 functions as an antagonist by inhibiting the hydrolytic activities of the receptor in rice and *Striga* species. These observations suggest that the butenolide group (D-ring) may be a more effective SL-modification site than the enol ether region in the development of a receptor antagonist. This suggestion is supported by the mechanism underlying SL perception, in which the nucleophilic attack site for the catalytic serine is the carbonyl group of the D-ring (Zhao et al. 2013, Yao et al. 2016) rather than the enol ether region (Mangnus and Zwanenburg 1992).

The ability to chemically control the functions of plant hormones would be useful for addressing biological questions in multiple plant species. For SLs, the receptor has been an attractive target for regulating SL signaling in plants, especially parasitic weeds. Thus, numerous SL receptor agonists have been developed both as chemical tools and as agrochemicals (e.g., suicide germination compounds). However, the development of antagonists has lagged behind that of agonists. The characterization of carba-SL compounds as novel antagonists confirmed that simple modifications of SL agonists can convert them into antagonists capable of inhibiting the hydrolytic activities of the receptors, which has potential implications beyond plant species. For example, carba-SLs inhibited D14 and ShHTL7 activities, and blocked SL signaling in rice as well as in a *Striga* species, although not dramatically. The absolute stereochemistry of carba-SLs should be determined to identify the biologically active isomers in each plant species. The results of this study provide useful lead compounds for designing and developing an ideal SL receptor antagonist.

Materials and Methods

Synthesis of carba-SLs (3–5)

General procedures

^{1}H NMR spectra were recorded with tetramethylsilane as the internal standard using a JEOLECA 500II (500 MHz) spectrometer (JEOL Ltd.). ^{13}C NMR and 2D-correlation NMR experimental spectra were recorded using a JEOLECA 500II (500 MHz). All peak assignments refer to the numbering in the structure of **GR24** (Fig. 1). High-resolution mass spectra were obtained with an AB SCIEX Triple TOF^{TM}5600 System (AB Sciex Pte. Ltd.). Column chromatography was performed using silica gel (Wakogel C-200, Wako Pure Chemical Industries, Ltd.).

(*E*)-3-(((3-methyl-4-oxocyclopent-2-en-1-yl)oxy)methylene)-3,3a,4,8b-tetrahydro-2H-indeno[1,2-b]furan-2-one, (±)-1′-carba-GR24 (3)

Sodium hydride (NaH, 60% in oil, 71 mg, 1.6 mmol) and methyl formate (0.5 mL, 8.0 mmol) under an atmosphere of Ar were added to a solution of ABC-ring compound **6** (70 mg, 0.40 mmol) in diethyl ether (5.5 mL). The mixture was stirred for 4 h at room temperature. After quenching with 1 M HCl (4 mL), it was then extracted with EtOAc (7 mL × 3), washed with brine and dried over Na_2SO_4. Then, the solvent was removed *in vacuo*. The white solid residue (147 mg) and K_2CO_3 (116 mg, 0.84 mmol) were dissolved in *N*-methylpyrrolidone (1 mL), and a solution of **7** (116 mg, 0.84 mmol) in *N*-methylpyrrolidone (0.5 mL) was added dropwise to the stirred mixture. The reaction mixture was stirred at room temperature for 30 min. After quenching with 1 M HCl (4 mL), it was extracted with EtOAc (7 mL × 3), washed with brine, dried over Na_2SO_4 and concentrated *in vacuo*. The residual oil was chromatographed on silica gel employing a stepwise elution with hexane and EtOAc. A portion of the 30% EtOAc eluate containing (±)-1′-carba-GR24 (**3**) was chromatographed on a Senshu PAK PEGASIL ODS SP100 HPLC column (250 × 20.0 mm, Senshu) and eluted under isocratic conditions using 70% MeOH in water containing 0.1% formic acid at a flow rate of 10 mL min^{-1}. A mixture of two inseparable diastereomers (8.3 mg, 7%), eluting as a single peak at 10.6 min, was collected. Subsequently, the diastereomeric mixture of (±)-1′-carba-GR24 (**3**) was chromatographed on a semi-preparative CHIRALPAK IC HPLC column (250 × 10.0 mm, Daicel) using isocratic elution with 70% EtOAc in hexane at a flow rate of 4.0 mL min^{-1}. The materials at t_R 5.5, 6.6, 8.8 and 15.9 min were collected as separable diastereomers and enantiomers (**3a**, **3b**, **3c** and **3d**, respectively).

3a and **3c** (enantiomers): ^{1}H NMR (500 MHz, $CDCl_3$) δ_H 1.89 (3H, dd, *J*=1.7 and 1.7 Hz, -CH_3), 2.48 (1H, dd, *J*=18.3 and 1.7 Hz, H-1′), 2.89 (1H, dd, *J*=18.3 and 6.3 Hz, H-1′), 3.08

(1H, dd, *J*=16.6 and 2.9 Hz, H-4), 3.40 (1H, dd, *J*=16.6 and 9.2 Hz, H-4), 3.91 (1H, m, H-3a), 5.19 (1H, m, H-2′), 5.94 (1H, d, *J*=8.0 Hz, H-8b), 7.23 (1H, d, *J*=7.4 Hz, H-5), 7.23 (1H, m, H-3′), 7.28 (1H, ddd, *J*=7.4, 7.4 and 1.1 Hz, H-7), 7.33 (1H, ddd, *J*=7.4, 7.4 and 1.1 Hz, H-6), 7.45 (1H, d, *J*=2.3 Hz, H-9), 7.50 (1H, d, *J*=7.4 Hz, H-8), ^{13}C NMR (125 MHz, $CDCl_3$): δ_C 10.2 (CH_3), 37.4 (C4), 38.9 (C3a), 41.4 (C1′), 80.0 (C2′), 85.7 (C8b), 110.6 (C3), 125.2 (C5), 126.5 (C8), 127.5 (C7), 130.0 (C6), 139.1 (C8b), 142.6 (C4a), 146.9 (C4′), 151.3 (C3′), 153.8 (C9), 172.0 (C2), 203.7 (C5′) (Supplementary Fig. S9). HRMS (*m/z*): $[M+H]^+$ calcd for $C_{18}H_{17}O_4$, 297.1121; found, 297.1113.

3b and **3d** (enantiomers): ^{1}H NMR (500 MHz, $CDCl_3$) δ_H 1.90 (3H, dd, *J*=1.7 and 1.1 Hz, -*CH*$_3$), 2.50 (1H, dd, *J*=18.9 and 2.3 Hz, H-1′), 2.91 (1H, dd, *J*=18.9 and 6.3 Hz, H-1′), 3.09 (1H, dd, *J*=16.6 and 2.9 Hz, H-4), 3.41 (1H, dd, *J*=16.6 and 9.2 Hz, H-4), 3.92 (1H, m, H-3a), 5.20 (1H, m, H-2′), 5.95 (1H, d, *J*=7.4 Hz, H-8b), 7.23 (1H, m, H-3′), 7.23 (1H, d, *J*=7.4 Hz, H-5), 7.28 (1H, dd, *J*=7.4 and 7.4 Hz, H-7), 7.34 (1H, ddd, *J*=7.4, 7.4 and 1.7 Hz, H-6), 7.46 (1H, d, *J*=2.3 Hz, H-9), 7.51 (1H, d, *J*=7.4 Hz, H-8), ^{13}C NMR (125 MHz, $CDCl_3$): δ_C 10.2 (CH_3), 37.3 (C4), 38.9 (C3a), 41.4 (C1′), 80.0 (C2′), 85.7 (C8b), 110.4 (C3), 125.1 (C5), 126.5 (C8), 127.4 (C7), 129.9 (C6), 139.1 (C8b), 142.6 (C4a), 146.9 (C4′), 151.3 (C3′), 153.9 (C9), 172.1 (C2), 203.8 (C5′) (Supplementary Fig. S10). HRMS (*m/z*): $[M+H]^+$ calcd for $C_{18}H_{17}O_4$, 297.1121; found, 297.1118.

4-(4-Bromophenoxy)-2-methylcyclopent-2-en-1-one, (±)-1′-carba-4BD (4)

4-Bromophenol (31 mg, 0.18 mmol) and triphenylphosphine (52 mg, 0.20 mmol) under an atmosphere of Ar were added to a solution of **8** (18 mg, 0.16 mmol) in toluene (0.9 mL). After stirring the mixture for 10 min at −10°C, diisopropyl azodicarboxylate (100 μL, 0.19 mmol) was added dropwise to the mixture. The reaction mixture was stirred for 3.5 h at the same temperature. After quenching with 5% aqueous $NaHCO_3$ solution (5 mL), it was then

extracted with EtOAc (8 mL × 3), washed with brine, dried over Na_2SO_4 and concentrated *in vacuo*. The residual oil was purified by silica gel chromatography with 3% acetone in hexane to obtain **4** (22 mg, 51%) as a colorless oil. ^{1}H NMR (500 MHz, $CDCl_3$): δ_H 1.87 (3H, dd, *J*=1.7 and 1.1 Hz, CH_3), 2.45 (1H, dd, *J*=18.3 and 1.7 Hz, H-1′), 2.90 (1H, dd, *J*=18.3 and 5.7 Hz, H-1′), 5.31 (1H, m, H-2′), 6.80 (2H, m, Ar), 7.31 (1H, m, H-3′), 7.41 (2H, m, Ar); ^{13}C NMR (125 MHz, $CDCl_3$): δ_C 10.1 (CH_3), 41.8 (C1′), 73.6 (C2′), 113.8 (Ar), 117.1 (Ar), 117.1 (Ar), 132.6 (Ar), 132.6 (Ar), 145.5 (C4′), 152.5 (C3′), 156.6 (Ar), 204.8 (C5′) (Supplementary Fig. S11). HRMS (*m/z*): $[M+H]^+$ calcd for $C_{12}H_{12}O_2Br$, 267.0015; found, 267.0018.**1-(4-Bromophenyl)but-3-en-2-ol (10)**

Aldehyde **9** (310 mg, 1.56 mmol) in anhydrous THF (8 mL) was cooled to −15°C under an atmosphere of Ar. Vinylmagnesium bromide (1 M solution in THF, 1.7 mL, 1.7 mmol) was then added slowly. The reaction mixture was stirred for further 60 min at the same temperature. After quenching with a saturated aqueous NH_4Cl solution (10 mL), it was extracted with EtOAc (20 mL × 3). The organic layer was washed with brine, dried over Na_2SO_4 and concentrated *in vacuo*. The residual oil was purified by silica gel chromatography with hexane-EtOAc stepwise to obtain **10** (93 mg, 26%) as a pale-yellow oil. ^{1}H NMR (500 MHz, $CDCl_3$): δ_H 1.58 (1H, d, *J*=4.0 Hz, -OH), 2.76 (1H, dd, *J*=13.7 and 8.0 Hz, CH_2CHOH), 2.82 (1H, dd, *J*=13.7 and 5.7 Hz, CH_2CHOH), 4.33 (1H, m, CH_2*CH*OH), 5.14 (1H, ddd, *J*=10.3, 1.7 and 1.1 Hz, CH=CH_2), 5.23 (1H, ddd, *J*=17.2, 1.7 and 1.1 Hz, CH=CH_2), 5.90 (1H, ddd, *J*=17.2, 10.3 and 6.3 Hz, *CH*=CH_2), 7.11 (2H, m, Ar), 7.43 (2H, m, Ar); ^{13}C NMR (125 MHz, $CDCl_3$): δ_C 43.0, 73.5, 115.3, 120.4, 131.3, 131.3, 131.5, 131.5, 136.8, 139.9. HRMS (*m/z*): $[M+Na]^+$ calcd for $C_{10}H_{11}OBrNa$, 248.9885; found, 248.9884.

1-(4-Bromophenyl)but-3-en-2-yl methacrylate (11)

Et_3N (115 µL 0.82 mmol), 4-DMAP (3.0 mg, 0.03 mmol) and methacryloyl chloride (80 µL 0.82 mmol) were added to a cooled (0°C) solution of alcohol **10** (93 mg, 0.41 mmol) in CH_2Cl_2 (4.5 mL). The reaction mixture was stirred for further 30 min at 0°C and then the ice bath was removed. The reaction mixture was stirred at room temperature for 2 h. After quenching with water (8 mL), it was extracted with EtOAc (10 mL × 3). The organic layer was washed with brine, dried over Na_2SO_4 and concentrated *in vacuo*. The residual oil was purified by silica gel chromatography with 2% EtOAc in hexane to obtain **11** (65 mg, 54%) as a colorless oil. ^{1}H NMR (500 MHz, $CDCl_3$): δ_H 1.91 (3H, s, CH_3), 2.90 (1H, dd, *J*=13.7 and 5.7 Hz, CH_2CH), 2.95 (1H, dd, *J*=13.7 and 6.9 Hz, CH_2CH), 5.17 (1H, d, *J*=10.3 Hz, CHCH=CH_2), 5.22 (1H, d, *J*=17.2 Hz, CHCH=CH_2), 5.48 (1H, m, CH_2*HC*), 5.55 (1H, dd, *J*=1.7 and 1.1 Hz, C=CH_2), 5.81 (1H, ddd, *J*=17.2, 10.3 and 6.3 Hz, CH*CH*=CH_2), 6.08 (1H, br s, C=CH_2), 7.08 (2H, m, Ar), 7.40 (2H, m, Ar); ^{13}C NMR (125 MHz, $CDCl_3$): δ_C 18.3, 40.3, 75.0, 117.2, 120.5, 125.6, 131.3, 131.3, 131.4, 131.4, 135.5, 135.8, 136.3, 166.4. HRMS (*m/z*): $[M+Na]^+$ calcd for $C_{14}H_{15}O_2BrNa$, 317.0148; found, 317.0148.

5-(4-Bromobenzyl)-3-methylfuran-2(5H)-one, (±)-7′-carba-4BD (5)

A CH_2Cl_2 solution (1 mL) of branched allylic ester **11** (45 mg, 0.15 mmol) was added to a solution of second generation Grubbs catalyst (7.3 mg, 6 mol%) in CH_2Cl_2 (10 mL). The reaction mixture was stirred at room temperature for 6.5 h. The solvent was evaporated *in vacuo*, and residual oil was purified by silica gel column chromatography with hexane-EtOAc stepwise to obtain **5** (25.5 mg, 63%) as a colorless solid. ^{1}H NMR (500 MHz, $CDCl_3$): δ_H 1.87 (3H, dd, *J*=2.3 and 1.7 Hz, -CH_3), 2.91 (1H, dd, *J*=14.3 and 6.3 Hz, H-7′), 2.99 (1H, dd, *J*=14.3 and 6.9 Hz, H-7′), 5.04 (1H, m, H-2′), 6.97 (1H, m, H-3′), 7.09 (2H, m, Ar), 7.44 (2H, m, Ar); ^{13}C NMR (125 MHz, $CDCl_3$): δ_C 10.7 (CH_3), 39.3 (C7′), 80.7 (C2′), 121.2 (Ar), 130.9 (C4′), 131.1 (Ar), 131.1 (Ar), 131.8 (Ar), 131.8 (Ar), 134.2 (Ar), 147.5 (C3′), 173.7 (C5′)

(Supplementary Fig. S12). HRMS (*m/z*): $[M+H]^+$ calcd for $C_{12}H_{11}O_2Br$, 267.0015; found, 267.0013.

Yeast two-hybrid assay

The Matchmaker Two-Hybrid System (Clontech) was used for the yeast two-hybrid assay. We used pGBK–D14 as the bait and pGAD–D53 as the prey (Nakamura et al. 2013). The *Saccharomyces cerevisiae* AH109 strain was transformed with the bait and prey plasmids and then grown in liquid medium for 2 days. The plate assays involving synthetic defined medium without histidine and adenine were completed according to a slightly modified manufacturer's protocol. Specifically, the medium contained various combinations of test compounds and 1 μM GR24.

D14 enzymatic in vitro assay

A reaction mixture containing 6 μg mL^{-1} purified D14, (±)-GR24 (10 μM final concentration), and inhibitors (4–128 μM in 5 μL DMSO) in PBS buffer (pH 7.7) was incubated at 30 °C for 20 min. Reactions were initiated by adding (±)-GR24 and then stopped by the addition of 50 μL 1 M HCl. The internal standard (5.0 ng 4-chloro-debranone) was added to the reaction mixture before the following extraction procedure. The enzyme products and residual (±)-GR24 were extracted with EtOAc (3 × 0.3 mL) and concentrated *in vacuo*. The dried sample was then dissolved in 25 μL MeOH, after which a 10-μL aliquot was analyzed in an HPLC system equipped with a PU 2080 HPLC pump (Jasco) and the MD1510 photodiode array detector (Jasco). The system was controlled using the ChromNAV (version 1.18.07) program (Jasco). The HPLC conditions were as follows: column: CAPCELL CORE C18 (150 × 4.6 mm, Shiseido); solvent: 45% MeOH in H_2O; flow rate: 1.0 mL min^{-1}; and detection wavelength: 254 nm. Enzyme activity was evaluated by determining the amount of

hydrolyzed GR24 in the control samples before each set of measurements. The IC_{50} values were calculated using the Enzyme Kinetics module of the SigmaPlot 14 program.

For the hydrolysis resistance test, a reaction mixture containing 12 μg mL^{-1} purified D14 and (±)-GR24, (±)-4BD or (±)-carba-SLs (10 μM final concentration) in PBS buffer (pH 7.7) was incubated at 30°C for 3 h. After adding 0.1 mL of 0.5 M HCl and 4-chloro-debranone, the enzyme products or residual (±)-carba-SLs were extracted with EtOAc (3 × 0.4 mL) and concentrated *in vacuo*. The dried sample was then dissolved in 25 μL MeOH, after which a 10-μL aliquot was analyzed by HPLC.

Yoshimulactone Green assay

The hydrolysis of YLG by D14 or HTL7 was analyzed using a modified version of a published procedure (Tsuchiya et al. 2015). Yoshimulactone Green (0.3 μM) was incubated with recombinant D14 (0.15 μM) or ShHTL7 (0.3 μM) in the absence or presence of carba-SL compounds (0.1, 0.3, 1, 3, 10, 30, or 100 μM) for 10 min. Fluorescence intensity was measured using the Appliskan plate reader (Thermo Fisher Scientific, Waltham, MA, USA), with excitation and detection wavelengths of 486 and 535 nm, respectively. The IC_{50} values were calculated using the Enzyme Kinetics module of the SigmaPlot 14 program.

Protein preparation

Rice D14 was produced in *E. coli* and purified as previously described (Nakamura et al. 2013). Briefly, the cDNA encoding rice D14 (residues 54−318) was inserted into the pET-49b expression vector (Merck-Millipore) for a subsequent expression in *E. coli* Rosetta (DE3) cells (Merck-Millipore). The cells were harvested, resuspended in extraction buffer [20 mM Tris-HCl (pH 8.5), 500 mM NaCl, 10% glycerol, and 3 mM dithiothreitol], and disrupted by sonication. The soluble fraction separated by centrifugation was purified using Glutathione Sepharose 4B resin (GE Healthcare) and a Resource S column (GE Healthcare). The purified

D14 was concentrated to 6.0 mg mL^{-1} in a buffer consisting of 20 mM MES-NaOH (pH 6.5), 300 mM NaCl, 10% glycerol, and 5 mM dithiothreitol.

Crystallization and structural analysis of the D14-D-ring–opened 7'-carba-4BD complex

The D14 protein (6.0 mg mL^{-1}) and 10 mM 7′-carba-4BD were mixed together and subjected to crystallization by the sitting drop vapor diffusion method. Crystals of the D14-D-ring–opened 7′-carba-4BD complex were obtained at 20 °C using a reservoir solution containing 100 mM HEPES (pH 7.5) and 8% PEG-20000. Crystals were soaked in a cryo-protectant solution containing 25% (v/v) ethylene glycol and then flash-cooled with a nitrogen-gas stream at 100 K. X-ray diffraction data were collected using an in-house X-ray diffractometer (Rigaku FR-E rotating-anode X-ray generator with R-AXIS VII imaging-plate detector) and processed with the XDS package (Kabsch 2010). The molecular replacement was completed using Phaser (McCoy et al. 2007) in PHENIX (Adams et al. 2010), with the apo-D14 structure (PDB code 3VXK) (Nakamura et al. 2013) as the initial model. Coot (Emsley and Cowtan 2004) was used to manually fit the protein models, and the structure was refined with PHENIX. The geometry of the final model was analyzed using RAMPAGE (Lovell et al. 2003). Additionally, the superposition and r.m.s.d. of the structures were calculated using the CCP4 program LSQKAB (Kabsch 1976). Figures for structures were prepared using PyMOL (DeLano, W. L. 2012). The X-ray data and refinement statistics are provided in Supplementary Table S1. The coordinates of the D14-D-ring–opened 7′-carba-4BD complex X-ray structure has been deposited in the Protein Data Bank (accession code 5YZ7).

Physiological assays for rice and Striga hermonthica

An SL-deficient rice (*Oryza sativa* L. ssp. *japonica* cv. Nipponbare) mutant, *d10-2*, was used for the rice tillering assay. Rice seeds were sterilized in 2.5% sodium hypochlorite solution containing 0.02% Tween-20 for 20 min. The seeds were washed five times with sterilized

water and then placed in tubes filled with water for a subsequent 2-day incubation at 25 °C in darkness. Germinated seeds were added to a hydroponic culture medium (Kamachi et al. 1991) solidified with 0.6% agar and then incubated at 25 °C under fluorescent light with a 16-h light/8-h dark photoperiod for 7 days. Each seedling was transferred to a glass vial filled with 12 mL sterilized hydroponic culture solution with or without an experimental compound, and grown under the same conditions for 7 days.

For the *Striga* species seed germination assay, *S. hermonthica* seeds were sterilized with 1% sodium hypochlorite solution containing 0.01% Tween-20 for 5 min. The seeds were washed five times with sterilized water and then added to 0.1% agar solution. Droplets of the solution were added to small, round, glass-fiber filters, which were then arranged in a Petri dish containing filter paper moistened with 1.2 mL sterilized water. The dishes were incubated at 30 °C in darkness for 7 days. The small filters with seeds were transferred to a 96-well plate, and 10 µL sterilized water or water containing an appropriate chemical was added to each well. After a 3-day incubation under the same conditions, the number of germinated seeds was counted.

Supplementary data

Supplementary data are available at PCP online.

PDB ID: The atomic coordinates of the D14-D-ring–opened 7′-carba-4BD complex have been deposited under accession code 5YZ7.

Funding

This work was supported in part by the Japan Society for the Promotion of Science KAKENHI (15J05877 to J.T. as well as 16H06736, 17J04676, and 17K15258 to K.H.), by a grant from the

Core Research for Evolutional Science and Technology Program of the Japan Science and Technology Agency, and by the Science and Technology Research Promotion program for agriculture, forestry, fisheries, and the food industry.

Disclosures

The authors have no conflicts of interest to declare.

Acknowledgments

We thank Prof. A. E. Babiker (Sudan University of Science and Technology) for providing the *S. hermonthica* seeds harvested in Sudan and Prof. J. Kyozuka (Tohoku University) for kindly providing the rice SL mutants. We thank Edanz Group (www.edanzediting.com/ac) for editing a draft of this manuscript.

References

Adams, P.D., Afonine, P. V., Bunkóczi, G., Chen, V.B., Davis, I.W., Echols, N., et al. (2010) PHENIX: A comprehensive Python-based system for macromolecular structure solution. *Acta Crystallogr Sect D Biol Crystallogr*. 66: 213–221.

Akiyama, K., Matsuzaki, K. and Hayashi, H. (2005) Plant sesquiterpenes induce hyphal branching in arbuscular mycorrhizal fungi. *Nature* 435: 824–827.

Baraldi, P.G., Pollini, G.P., Simoni, D., Zanirato, V., Barco, A., and Benetti, S. (1986) A Facile, Efficient Synthesis of 2-substituted-4-Hydroxy- 2-cyclopenten-1-ones. *Synthesis (Stuttg)*. 1986: 781–782.

Brewer, P.B., Koltai, H., and Beveridge, C.A. (2013) Diverse roles of strigolactones in plant development. *Mol Plant*. 6: 18–28.

Calad, S.A. and Woerpel, K.A. (2007) Formation of chiral quaternary carbon stereocenters using silylene transfer reactions: enantioselective synthesis of (+)-5-epi-acetomycin. *Org Lett*. 9: 1037–40.

Conn, C.E., Bythell-douglas, R., Neumann, D., Yoshida, S., Whittington, B., Westwood, J.H., et al. (2015) Convergent evolution of strigolactone perception enabled host detection in parasitic plants. *Science*. 349: 540–543.

DeLano, W. L. (2012) *The PyMOL Molecular Graphics System*, version 1.8.6.0, Schroedinger, LLC, New York.

de Saint Germain, A., Bonhomme, S., Boyer, F.D., and Rameau, C. (2013) Novel insights into strigolactone distribution and signalling. *Curr Opin Plant Biol*. 16: 583–589.

de Saint Germain, A., Clavé, G., Badet-Denisot, M.-A., Pillot, J.-P., Cornu, D., Le Caer, J.-P., et al. (2016) An histidine covalent receptor and butenolide complex mediates strigolactone perception. *Nat Chem Biol*. 12: 787–794.

Ehrhardt, D.W., Biol, N.C., Toh, S., Holbrook-smith, D., Stogios, P.J., Onopriyenko, O., et al. (2015) Structure-function analysis identifies highly sensitive strigolactone receptors in Striga. *Science* 350: 203–207.

Ejeta, G. (2007) THE *STRIGA* SCOURGE IN AFRICA: A GROWING PANDEMIC. In *Integrating New Technologies for Striga Control*. pp. 3–16 WORLD SCIENTIFIC.

Eleftheriadis, N., Poelman, H., Leus, N.G.J., Honrath, B., Neochoritis, C.G., Dolga, A., et al. (2016) Design of a novel thiophene inhibitor of 15-lipoxygenase-1 with both anti-inflammatory and neuroprotective properties. *Eur J Med Chem*. 122: 786–801.

Emsley, P., and Cowtan, K. (2004) Coot: Model-building tools for molecular graphics. *Acta Crystallogr Sect D Biol Crystallogr*. 60: 2126–2132.

Fukui, K., Ito, S., Ueno, K., Yamaguchi, S., Kyozuka, J., and Asami, T. (2011) New branching inhibitors and their potential as strigolactone mimics in rice. *Bioorg Med Chem Lett*. 21: 4905–8.

Gomez-Roldan, V., Fermas, S., Brewer, P.B., Puech-Pagès, V., Dun, E.A., Pillot, J.-P., et al. (2008) Strigolactone inhibition of shoot branching. *Nature*. 455: 189–194.

Hamiaux, C., Drummond, R.S.M., Janssen, B.J., Ledger, S.E., Cooney, J.M., Newcomb, R.D., et al. (2012) DAD2 is an α/β hydrolase likely to be involved in the perception of the plant branching hormone, strigolactone. *Curr Biol*. 22: 2032–6

Hamiaux, C., Drummond, R.S.M., Luo, Z., Lee, H.W., Sharma, P., Janssen, B.J., et al. (2018) Inhibition of strigolactone receptors by *N-phenylanthranilic* acid derivatives: structural and functional insights. *J Biol Chem*. In press.

Holbrook-smith, D., Toh, S., Tsuchiya, Y., and Mccourt, P. (2016) Small-molecule antagonists of germination of the parasitic plant Striga hermonthica. *Nat Chem Biol*. 12: 724–729.

Jiang, L., Liu, X., Xiong, G., Liu, H., Chen, F., Wang, L., et al. (2013) DWARF 53 acts as a repressor of strigolactone signalling in rice. *Nature*. 504: 401–405.

Kabsch, W. (1976) A solution for the best rotation to relate two sets of vectors. *Acta Crystallogr Sect A*. A32: 922–923.

Kabsch, W. (2010) Xds. *Acta Crystallogr Sect D Biol Crystallogr*. 66: 125–132.

Kamachi, K., Yamaya, T., Mae, T., and Ojima, K. (1991) A Role for Glutamine Synthetase in the Remobilization of Leaf Nitrogen during Natural Senescence in Rice Leaves. *Plant Physiol*. 96: 411–417.

Lovell, S.C., Davis, I.W., Adrendall, W.B., de Bakker, P.I.W., Word, J.M., Prisant, M.G., et al. (2003) Structure validation by C alpha geometry: phi,psi and C beta deviation. *Proteins-Structure Funct Genet*. 50: 437–450.

Louvel, J., Carvalho, J.F.S., Yu, Z., Soethoudt, M., Lenselink, E.B., Klaasse, E., et al. (2013) Removal of human ether-à-go-go related gene (hERG) K+ channel affinity through rigidity: a case of clofilium analogues. *J Med Chem*. 56: 9427–40.

Lumba, S., Bunsick, M., and McCourt, P. (2017) Chemical genetics and strigolactone perception. *F1000Research*. 6: 975.

Mangnus, E.M., Dommerholt, F.J., Jong, R.L.P.D. and Zwanenburg, B. (1992) Improved synthesis of strigol analog GR24 and evaluation of the biological activity of its diastereomers. *J. Agric. Food Chem.* 40: 1230–1235.

Mangnus, E.M., and Zwanenburg, B. (1992) Tentative molecular mechanism for germination stimulation of Striga and Orobanche seeds by strigol and its synthetic analogs. *J Agric Food Chem*. 40: 1066–1070.

Mashita, O., Koishihara, H., Fukui, K., Nakamura, H., and Asami, T. (2016) Discovery and identification of 2-methoxy-1-naphthaldehyde as a novel strigolactone-signaling inhibitor. *J Pestic Sci*. 41: 71–78.

McCoy, A.J., Grosse-Kunstleve, R.W., Adams, P.D., Winn, M.D., Storoni, L.C., and Read, R.J. (2007) Phaser crystallographic software. *J Appl Crystallogr*. 40: 658–674.

Nakamura, H., Xue, Y.-L., Miyakawa, T., Hou, F., Qin, H.-M., Fukui, K., et al. (2013) Molecular mechanism of strigolactone perception by DWARF14. *Nat Commun*. 4: 2613.

Nakamura, H., and Asami, T. (2014) Target sites for chemical regulation of strigolactone signaling. *Front Plant Sci*. 5: 1–9.

Naora, H., Ohnuki, T., and Nakamuka, A. (1988) A New Method of Synthesizing 7-(2-Hydroxy-5-oxo-1-cyclopentenyl)heptanoic Acid and Related Compounds. *Bull Chem Soc Jpn*. 61: 2401–2404.

Nardini M. & Dijkstra B. W. (1999) α/β hydrolase fold enzymes: the family keeps growing. *Curr. Opin. Struct. Biol.* 9: 732–737.

Seto, Y., and Yamaguchi, S. (2014) Strigolactone biosynthesis and perception. *Curr Opin Plant Biol*. 21: 1–6.

Thuring, J. W. J. F.; Bitter, H. H.; de Kok, M. M.; Nefkens, G. H. L.; van Riel, A. M. D. A.; Zwanenburg, B. (1997a) N-Pthaloylglycine-Derived Strigol Analogues. Influence of the D-Ring on Seed Germination Activity of the Parasitic Weeds Striga hermonthica and Orobanche crenata. *J Agric Food Chem*. 45: 2284–2290.

Thuring, J.W.J.F., Nefkens, G.H.L., and Zwanenburg, B. (1997b) Synthesis and Biological Evaluation of the Strigol Analogue Carba-GR24. *J Agric Food Chem*. 45: 1409–1414.

Tsuchiya, Y., Yoshimura, M., Sato, Y., Kuwata, K., Toh, S., Holbrook-Smith, D., et al. (2015) Probing strigolactone receptors in Striga hermonthica with fluorescence. *Science* 349: 864–868.

Umehara, M., Hanada, A., Yoshida, S., Akiyama, K., Arite, T., Takeda-Kamiya, N., et al. (2008) Inhibition of shoot branching by new terpenoid plant hormones. *Nature*. 455: 195–200.

Umehara, M., Cao, M., Akiyama, K., Akatsu, T., Seto, Y., Hanada, A., et al. (2014) Structural requirements of strigolactones for shoot branching inhibition in rice and arabidopsis. *Plant Cell Physiol*. 56: 1059–1072.

Wang, L., Wang, B., Jiang, L., Liu, X., Li, X., Lu, Z., et al. (2015) Strigolactone Signaling in Arabidopsis Regulates Shoot Development by Targeting D53-Like SMXL Repressor Proteins for Ubiquitination and Degradation. *Plant Cell*. 27: 3128–3142.

Waters, M.T., Gutjahr, C., Bennett, T., and Nelson, D.C. (2017) Strigolactone Signaling and Evolution. *Annu Rev Plant Biol*. 68: 291–322.

Xie, X., Yoneyama, K., and Yoneyama, K. (2010) The Strigolactone Story. *Annu Rev Phytopathol*. 48: 93–117.

Xiang, H., Yao, R., Quan, T., Wang, F., Chen, L., Du, X., et al. (2017) Simple β-lactones are potent irreversible antagonists for strigolactone receptors. *Cell Res*. 27: 1525–8.

Yao, R., Ming, Z., Yan, L., Li, S., Wang, F., Ma, S., et al. (2016) DWARF14 is a non-canonical hormone receptor for strigolactone. *Nature*. 536: 469–73.

Yao, R., Wang, F., Ming, Z., Du, X., Chen, L., Wang, Y., et al. (2017) ShHTL7 is a non-canonical receptor for strigolactones in root parasitic weeds. *Cell Res*. 27: 838–841.

Zhao, L.-H., Zhou, X.E., Wu, Z.-S., Yi, W., Xu, Y., Li, S., et al. (2013) Crystal structures of two phytohormone signal-transducing α/β hydrolases: karrikin-signaling KAI2 and strigolactone-signaling DWARF14. *Cell Res*. 23: 436–9.

Zhao, L.-H., Zhou, X.E., Yi, W., Wu, Z., Liu, Y., Kang, Y., et al. (2015) Destabilization of strigolactone receptor DWARF14 by binding of ligand and E3-ligase signaling effector DWARF3. *Cell Res*. 25: 1219–1236.

Zhou, F., Lin, Q., Zhu, L., Ren, Y., Zhou, K., Shabek, N., et al. (2013) D14–SCFD3-dependent degradation of D53 regulates strigolactone signalling. *Nature*. 504: 406–410.

Zwanenburg, B., Nayak, S.K., Charnikhova, T. V, and Bouwmeester, H.J. (2013) New strigolactone mimics: structure-activity relationship and mode of action as germinating stimulants for parasitic weeds. *Bioorg Med Chem Lett*. 23: 5182–6.

Figure legends

Fig. 1 Structures of (±)-GR24, (±)-4BD, and (±)-carba-SL compounds.

Fig. 2 Synthesis of carba-SL compounds. (A) Synthesis of (±)-1′-carba-GR24. Reagents: (i) 1) NaH, methyl formate and diethyl ether; 2) compound **7**, K_2CO_3 and NMP. (B) Synthesis of (±)-1′-carba-4BD. Reagents: (i) 4-bromophenol, DIAD, Ph_3P and toluene. (C) Synthesis of (±)-7′-carba-4BD. Reagents: (i) vinylmagnesium bromide and THF; (ii) methacryloyl chloride, 4-DMAP, Et_3N, and CH_2Cl_2; (iii) second generation Grubbs catalyst and CH_2Cl_2.

Fig. 3 Effects of carba-SLs on the tiller bud outgrowth of the SL-deletion *d10-2* rice mutant. The length of the second tillers of 9-d-old *d10-2* mutants treated with 0.1 μM (±)-GR24 and 10 μM (±)-1′-carba-GR24 (A), (±)-1′-carba-4BD (B) or (±)-7′-carba-4BD (C). Data are presented as the averages from three (A and B) or two (C) independent experiments (n = 6 each; error bars represent the standard errors). Values marked with different letters were statistically significantly different between the treatments (P-value < 0.01, Tukey's test).

Fig. 4 Carba-SLs were not cleaved by D14. (A) Enzymatic degradation of (±)-GR24, (±)-1′-carba-GR24 and (±)-7′-carba-4BD by D14. (B) Enzymatic production of 4-bromophenol by the hydrolysis of (±)-4BD or (±)-1′-carba-4BD. Each test compound (10 μM) was incubated with or without D14 (n = 3; error bars represent the standard deviations).

Fig. 5 Inhibitory effects of carba-SLs on D14 hydrolytic activity. Relative fluorescence of the YLG probe in the presence of purified D14 and increasing concentrations of (±)-1′-carba-GR24, (±)-1′-carba-4BD, (±)-7′-carba-4BD, (±)-GR24 or (±)-4BD (n = 3; error bars represent the standard deviations). The listed IC_{50} values are the averages from three experiments.

Fig. 6 Effects of carba-SLs on the interaction between D14 and D53. (A) Growth of AH109 yeast cells transformed independently with pGBK-D14 and pGAD-D53 on synthetic defined medium without histidine and adenine but supplemented with test compounds. (B) Inhibitory activity of each test compound against the GR24-induced interaction between D14 and D53. Assays were conducted in the absence (A) or presence (B) of 1 μM (±)-GR24 and 1, 10 and 50 μM (±)-1′-carba-GR24, (±)-1′-carba-4BD or (±)-7′-carba-4BD. The yeast solutions and their 1/10 dilutions were pipetted onto plates.

Fig. 7 Crystal structure of D14 in complex with D-ring-opened 7′-carba-4BD. (A) Overall structure of D-ring-opened 7′-carba-4BD-bound D14 in three different orientations. The bound D-ring-opened 7′-carba-4BD molecule is depicted in orange with van der Waals surfaces, and the pocket surface is shown in blue. (B) Binding site of D-ring-opened 7′-carba-4BD in the catalytic pocket of D14. D-ring-opened 7′-carba-4BD is shown as a stick model (orange) along with the $2F_o-F_c$ map contoured at 1.0 σ (gray). The residues involved in the interaction with D-ring-opened 7′-carba-4BD (< 4.5 Å) are represented in a line model. Water molecules are shown as red balls, and the blue broken line indicates a hydrogen bond. (C) Comparison of the ligand-binding modes of D-ring-opened 7′-carba-4BD-bound D14 (green) and GR24-bound D14 (PDB code 5DJ5) (blue). The orientation and structural representation are the same as in B. The bound GR24 molecule is shown as a yellow stick model.

Fig. 8 Antagonistic effects of carba-SLs on a *Striga* species. (A) Conditioned *Striga hermonthica* seeds were treated with acetone (Mock) or the indicated concentrations of carba-SLs in the presence of 10 nM (±)-GR24. The germination rate was measured after 3 d (*n* = 3; error bars represent the standard errors). (B) Inhibitory effects of carba-SLs on ShHTL7's hydrolytic activity. Relative fluorescence of the YLG probe in the presence of purified ShHTL7 at increasing concentrations of (±)-1′-carba-GR24, (±)-1′-carba-4BD or (±)-7′-carba-4BD (*n* = 3; error bars represent the standard deviations). The listed IC_{50} values are the averages from three experiments.

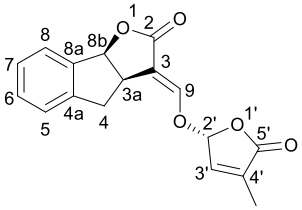

(±)-GR24 (**1**)

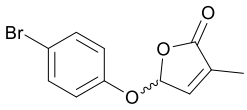

(±)-4BD (**2**)

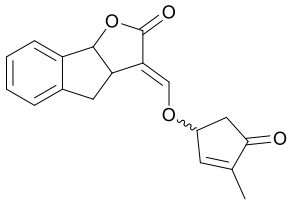

(±)-1'-carba-GR24 (**3**)

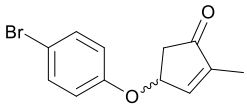

(±)-1'-carba-4BD (**4**)

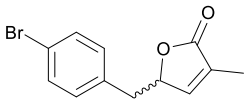

(±)-7'-carba-4BD (**5**)

Fig. 1 Structures of (±)-GR24, (±)-4BD, and (±)-carba-SL compounds.

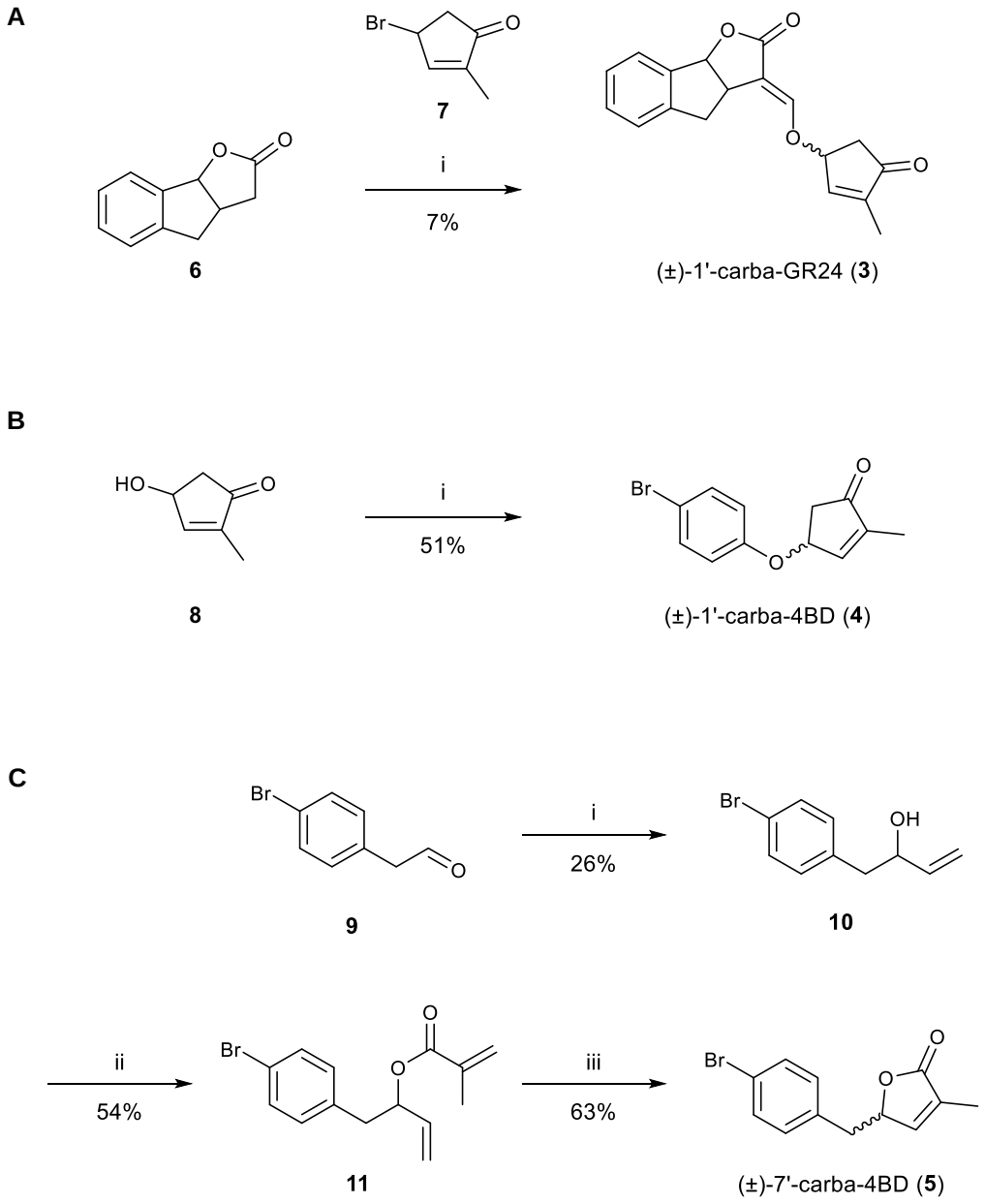

Fig. 2 Synthesis of carba-SL compounds. (A) Synthesis of (±)-1′-carba-GR24. Reagents: (i) 1) NaH, methyl formate and diethyl ether; 2) compound **7**, K_2CO_3 and NMP. (B) Synthesis of (±)-1′-carba-4BD. Reagents: (i) 4-bromophenol, DIAD, Ph_3P, and toluene. (C) Synthesis of (±)-7′-carba-4BD. Reagents: (i) vinylmagnesium bromide and THF; (ii) methacryloyl chloride, 4-DMAP, Et_3N, and CH_2Cl_2; (iii) second generation Grubbs catalyst and CH_2Cl_2.

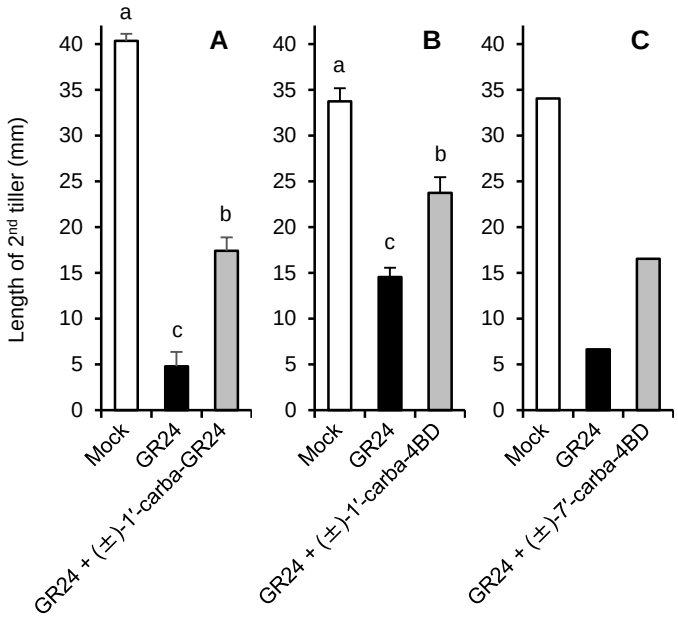

Fig. 3 Effects of carba-SLs on the tiller bud outgrowth of the SL-deletion *d10-2* mutant. The length of the second tillers of 9-day-old rice *d10-2* mutants treated with 0.1 μM (±)-GR24 and 10 μM (±)-1′-carba-GR24 (A), (±)-1′-carba-4BD (B), or (±)-7′-carba-4BD (C). Data are presented as the averages from three (A and B) or two (C) independent experiments (n = 6 each; error bars represent the standard error). Values marked with different letters differed significantly between the treatments (P-value < 0.01, Tukey's test).

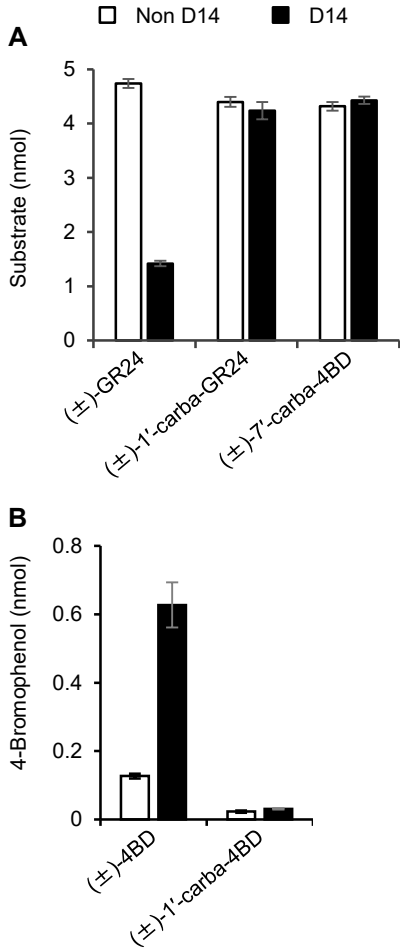

Fig. 4 Carba-SLs were not cleaved by D14. (A) Enzymatic degradation of (±)-GR24, (±)-1′-carba-GR24, and (±)-7′-carba-4BD by D14. (B) Enzymatic production of 4-bromophenol by the hydrolysis of (±)-4BD or (±)-1′-carba-4BD. Each test compound (10 μM) was incubated with or without D14 (*n* = 3; error bars represent the standard deviation).

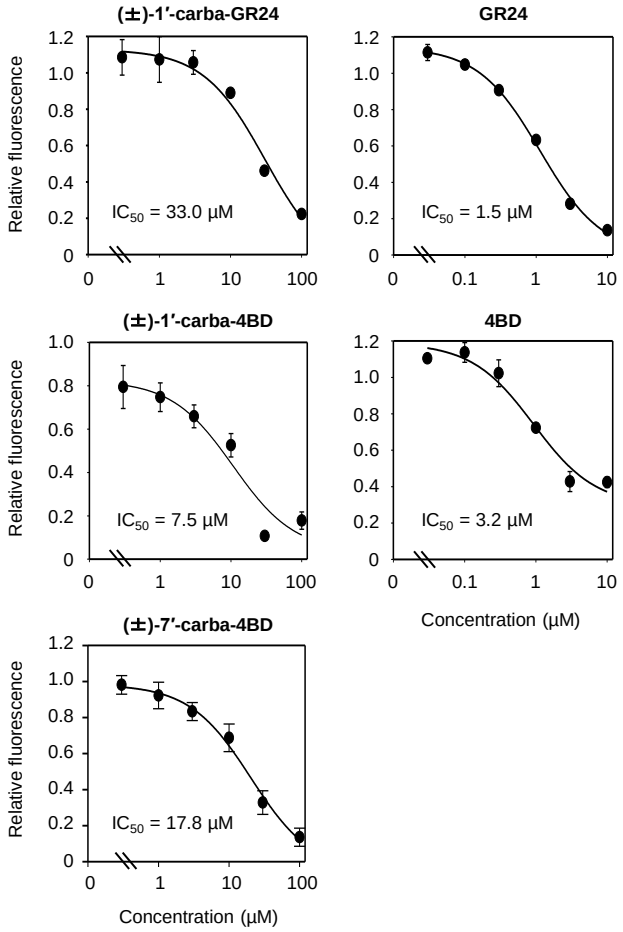

Fig. 5 Inhibitory effects of carba-SLs on D14 hydrolytic activity. Relative fluorescence of the YLG probe in the presence of purified D14 at increasing concentrations of (±)-1′-carba-GR24, (±)-1′-carba-4BD, (±)-7′-carba-4BD, (±)-GR24, and (±)-4BD (*n* = 3; error bars represent the standard deviation). The listed IC_{50} values are the averages from three experiments.

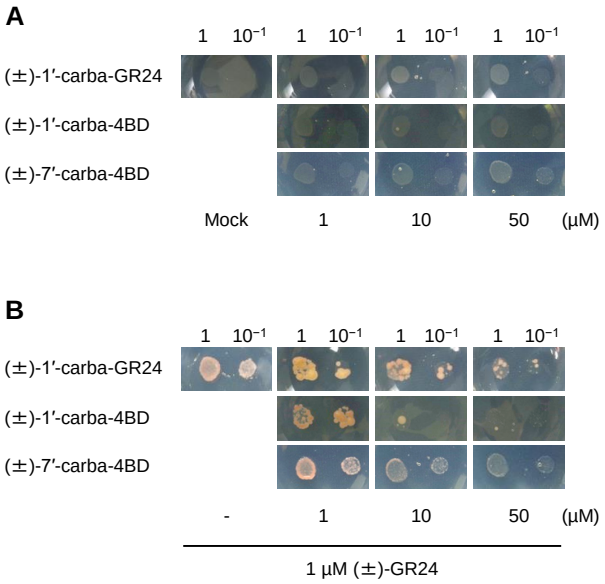

Fig. 6 Effects of carba-SLs on the interaction between D14 and D53. (A) Growth of AH109 yeast cells transformed with pGBK-D14 and pGAD-D53 on synthetic defined medium without histidine and adenine, but supplemented with test compounds. (B) Inhibitory activity of each test compound against the GR24-induced interaction between D14 and D53. Assays were conducted in the absence (A) or presence (B) of 1 μM (±)-GR24 and 1, 10, and 50 μM (±)-1′-carba-GR24, (±)-1′-carba-4BD, and (±)-7′-carba-4BD. The yeast solution and its 1/10 dilution were pipetted onto the plates.

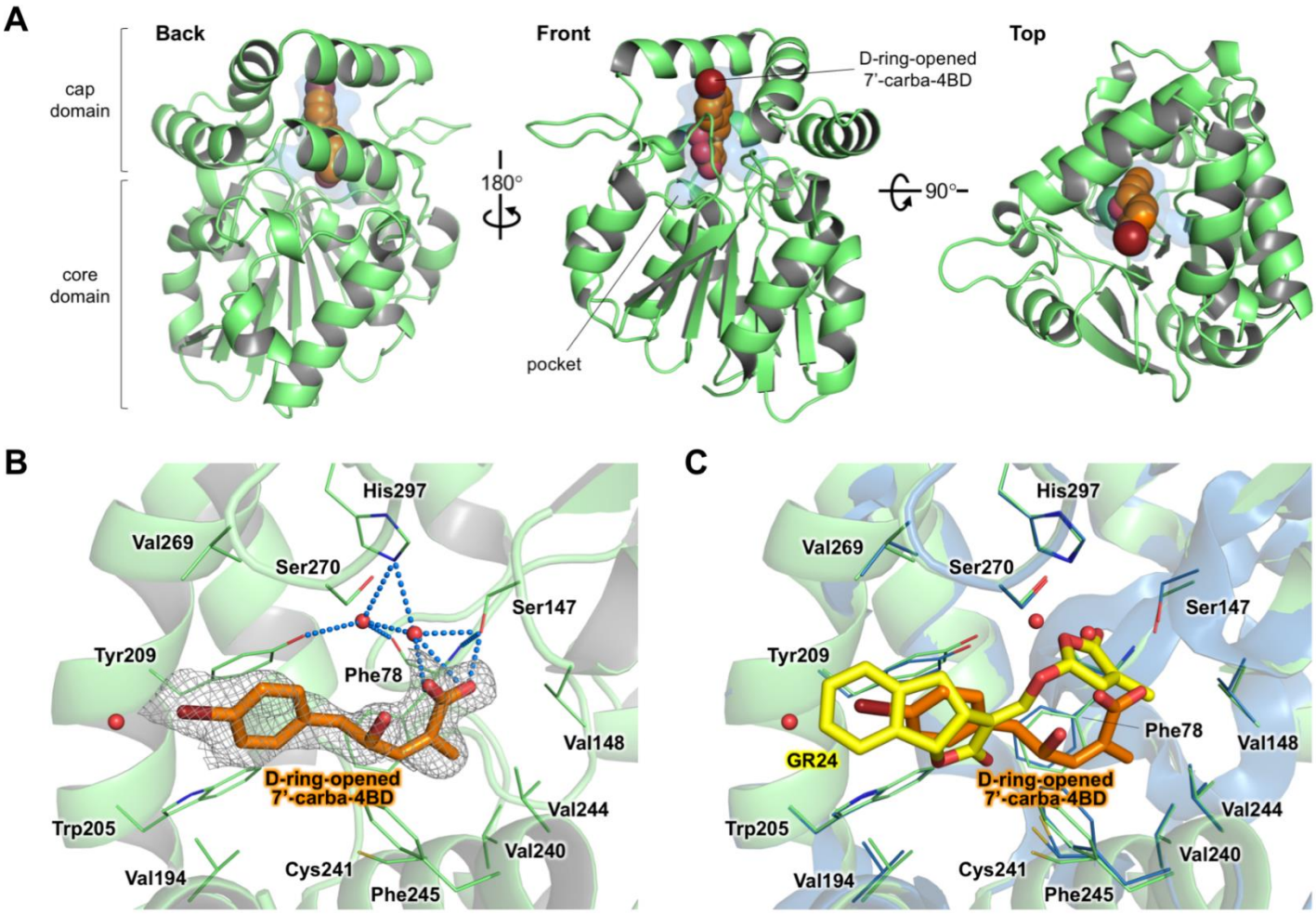

Fig. 7 Crystal structure of D14 in complex with D-ring–opened 7′-carba-4BD. (A) Overall structure of D-ring–opened 7′-carba-4BD–bound D14 in three different orientations. The bound D-ring–opened 7′-carba-4BD molecule is depicted in orange with van der Waals surfaces, and the pocket surface is shown in blue. (B) Binding site of D-ring–opened 7′-carba-4BD in the catalytic pocket of D14. D-ring–opened 7′-carba-4BD is shown as a stick model (orange) along with the 2*F*o-*F*c map contoured at 1.0 σ (gray). The residues involved in the interaction with D-ring–opened 7′-carba-4BD (< 4.5 Å) are represented by a line model. Water molecules are shown as red balls, and the blue broken line indicates a hydrogen bond. (C) Comparison of the ligand-binding modes of D-ring–opened 7′-carba-4BD–bound D14 (green) and GR24-bound D14 (PDB code 5DJ5) (blue). The orientation and structural representation are the same as in B. The bound GR24 molecule is shown as a yellow stick model.

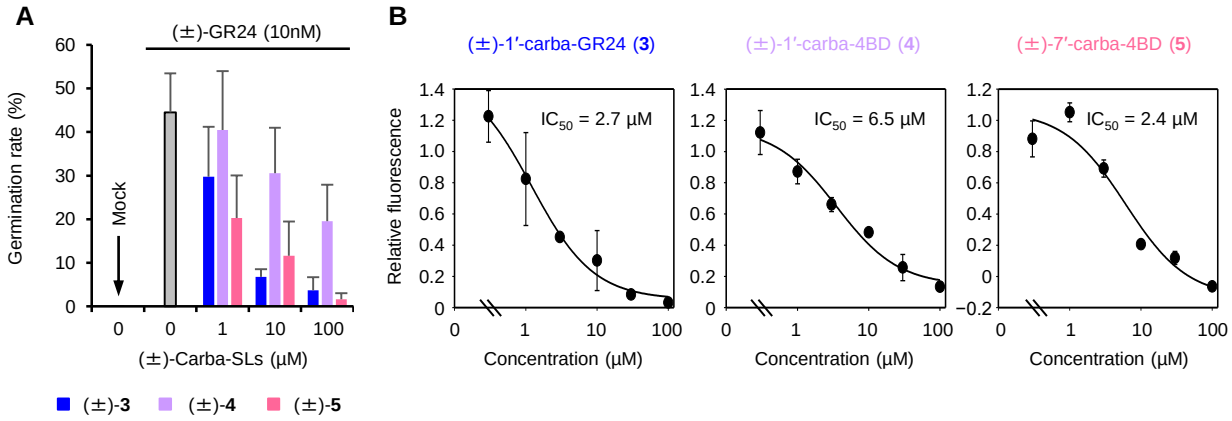

Fig. 8 Antagonistic effects of carba-SLs on a *Striga* species. (A) Conditioned *Striga hermonthica* seeds were treated with acetone (Mock) or the indicated concentrations of carba-SLs in the presence of 10 nM (±)-GR24. The germination rate was measured after 3 days (n = 3; error bars represent the standard error). (B) Inhibitory effects of carba-SLs on ShHTL7 hydrolytic activity. Relative fluorescence of the YLG probe in the presence of purified ShHTL7 at increasing concentrations of (±)-1′-carba-GR24, (±)-1′-carba-4BD, and (±)-7′-carba-4BD (n = 3; error bars represent the standard deviation). The listed IC_{50} values are the averages from three experiments.

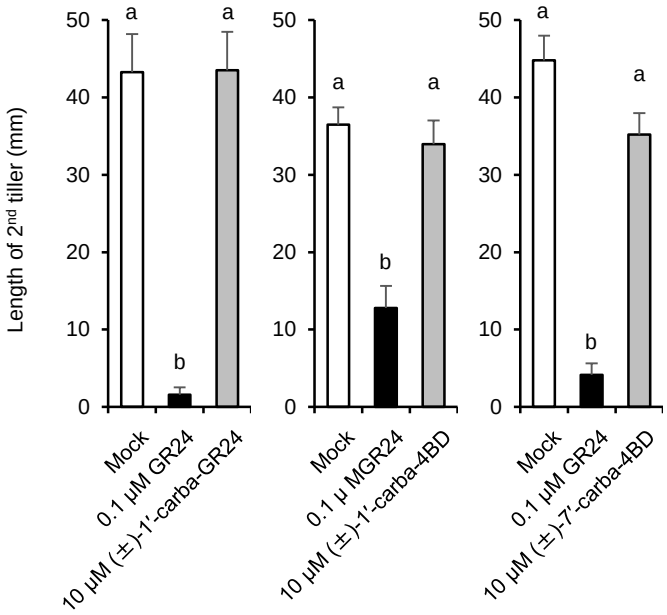

Fig. S1 Carba-SLs did not inhibit shoot branching in the rice *d10-2* mutant. The length of the second tillers of 2-week-old *d10-2* mutants treated with 0.1 μM (±)-GR24 or 10 μM carba-SLs (n = 6 each; error bars represent the standard error). Values marked with different letters differed significantly between the treatments (P-value < 0.01, Tukey's test).

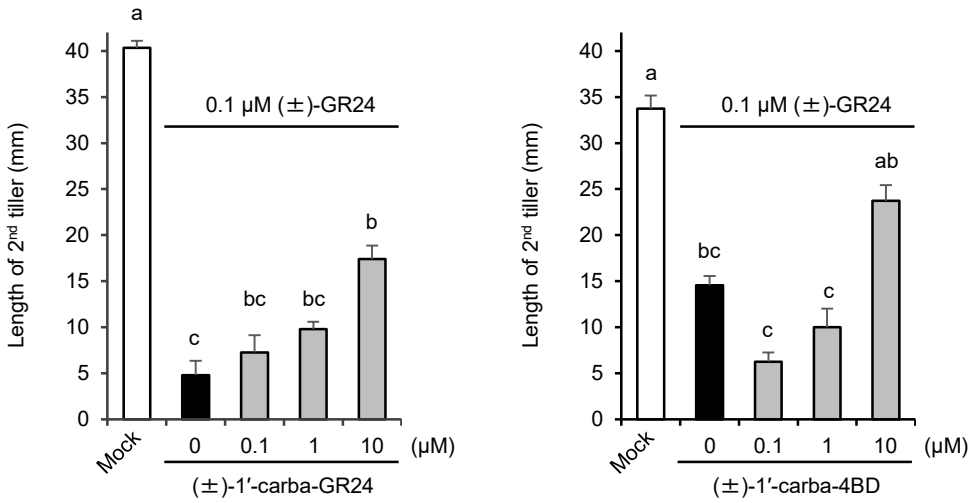

Fig. S2 Effects of (±)-1′-carba-GR24 and (±)-1′-carba-4BD on the tiller bud outgrowth of the SL-deletion *d10-2* mutant. The length of the second tillers of 9-day-old rice *d10-2* mutants treated with 0.1 μM (±)-GR24 and various concentration (0, 0.1, 1 and 10 μM) of (±)-carba-GR24 (A) and (±)-1′-carba-4BD (B). Data are presented as the averages from three independent experiments (n = 6 each; error bars represent the standard error). Values marked with different letters differed significantly between the treatments (P-value < 0.01, Tukey's test).

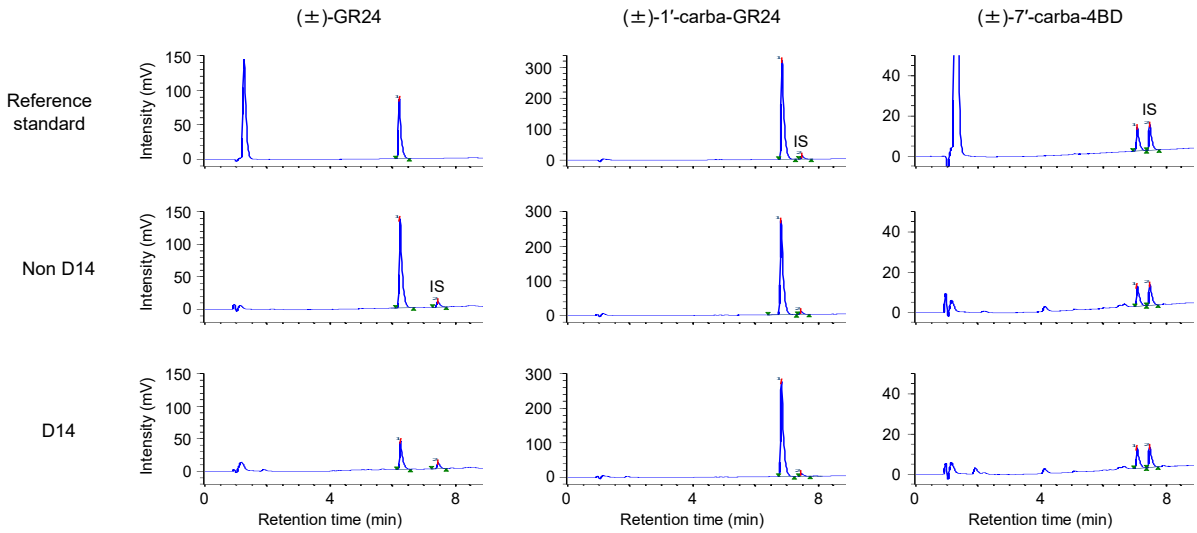

Fig. S3 HPLC data for quantification of the residual substrates, related to Fig. 4A. The HPLC conditions were as follows: column: CAPCELL CORE C18 (150 × 4.6 mm, Shiseido); solvent: linear gradient from 40% to 90% MeOH in water in 9 minutes; flow rate: 1.0 mL min^{-1}; and detection wavelength: 254 nm. The retention times of (±)-GR24, (±)-1′-carba-GR24 and (±)-carba-4BD are 6.2, 6.8 and 7.1 min, respectively.

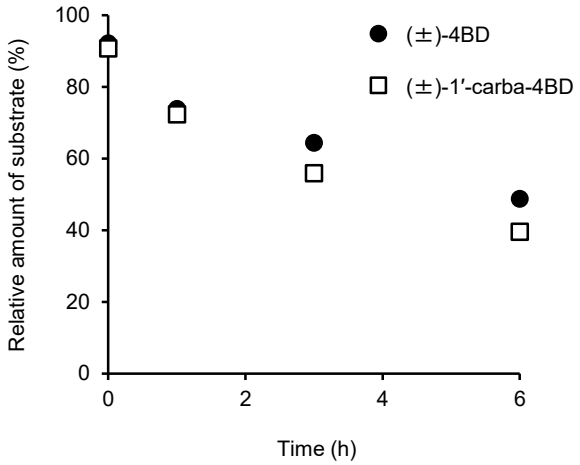

Fig. S4 Chemical stability of (±)-4BD and (±)-1′-carba-4BD in PBS buffer (pH 7.7) at 30 ° C.

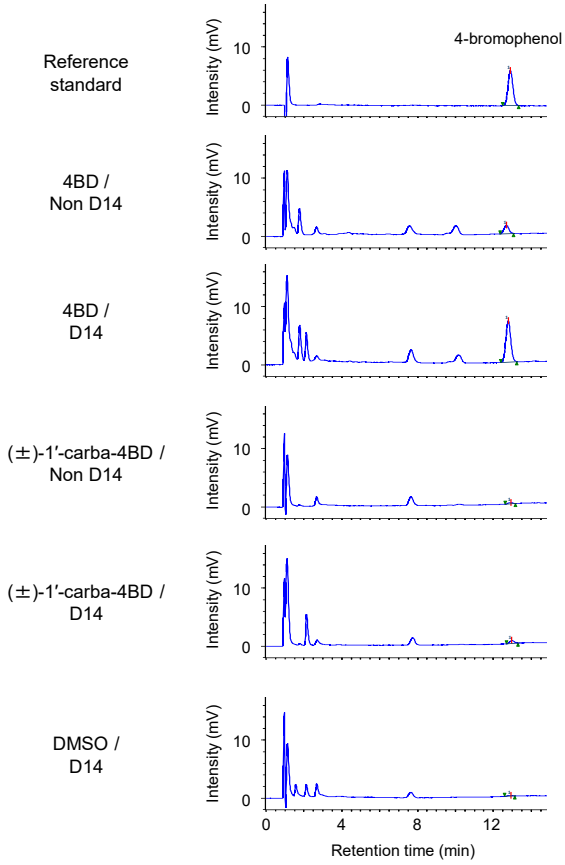

Fig. S5 HPLC data for quantification of the enzymatic product, 4-bromophenol, related to Fig. 4B. The HPLC conditions were as follows: column: CAPCELL CORE C18 (150 × 4.6 mm, Shiseido); solvent: 35% MeOH in water; flow rate: 1.0 mL min^{-1}; and detection wavelength: 230 nm. The retention time of 4-bromophenol is 12.9 min.

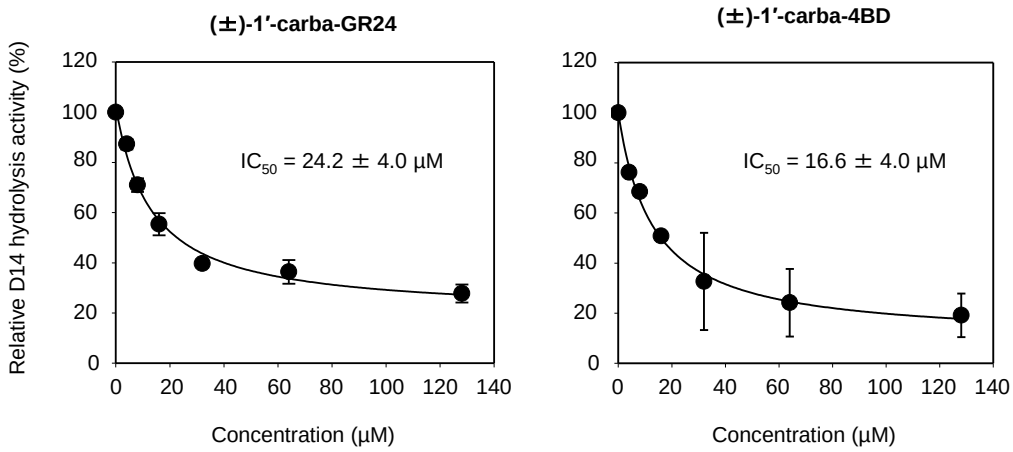

Fig. S6 Inhibitory effects of (±)-1′-carba-GR24 and (±)-1′-carba-4BD on the hydrolytic cleavage of (±)-GR24 by D14. Assays were completed in the presence of 10 μM (±)-GR24 and various concentrations (0–128 μM) of (±)-1′-carba-GR24 or (±)-1′-carba-4BD. The D14 protein was added at a final concentration of 6 μg mL^{-1} (n = 3; error bars represent the standard deviation). The listed IC_{50} values are the averages from three experiments.

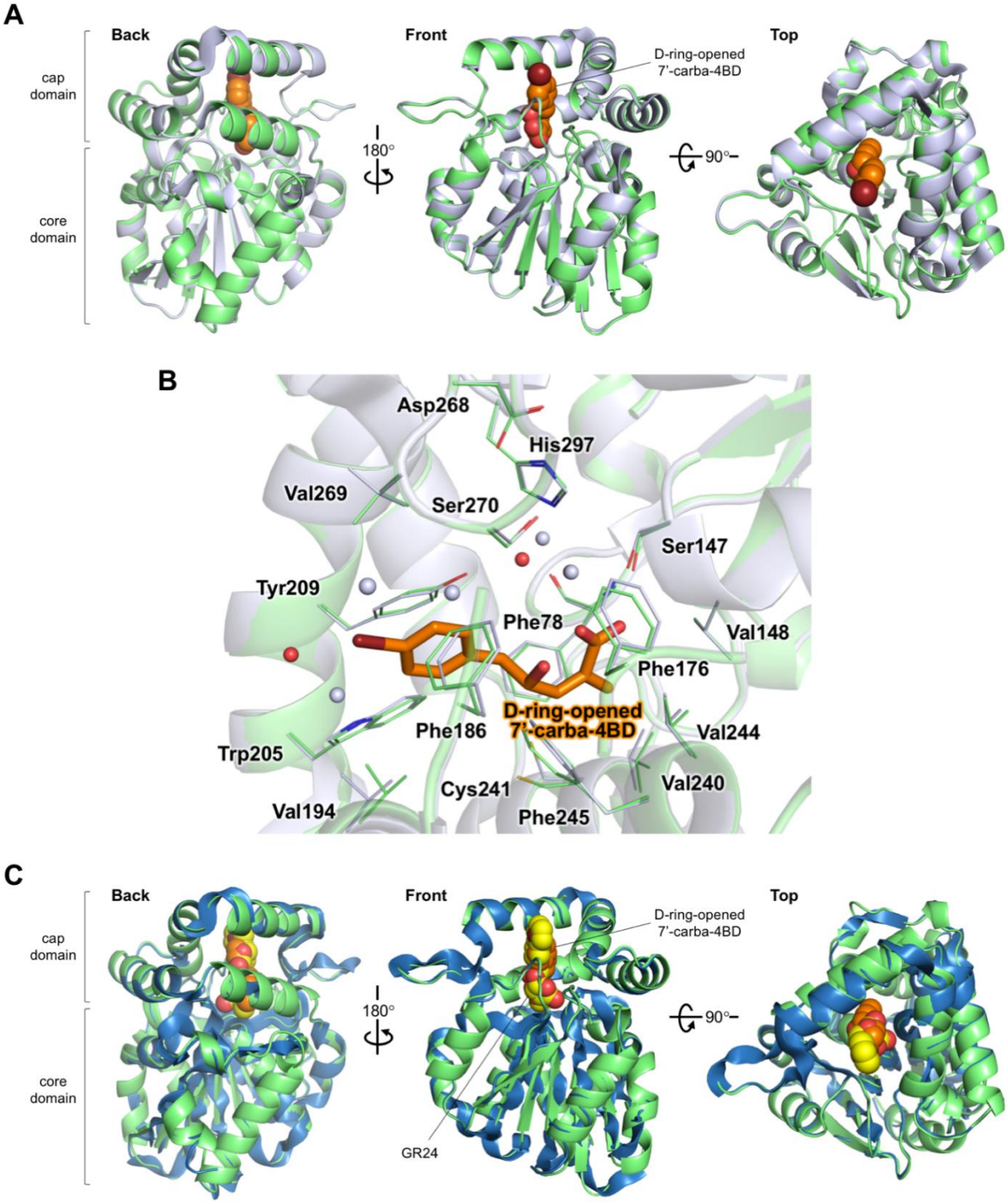

Fig. S7 Structural comparison. (A) Superposed structure of D-ring–opened 7′-carba-4BD–bound D14 (green) and apo-D14 (PDB code 3VXK) (white) in three different orientations. The bound D-ring–opened 7′-carba-4BD molecule is depicted in orange with van der Waals surfaces. The r.m.s.d. for the Cα atoms was 0.23 Å. (B) Magnified view of the D-ring–opened 7′-carba-4BD binding site in A. The orientation and structural representation are the same as in Fig. 7B and C. Water molecules from apo-D14 are shown as white balls. (C) Superposed structure of D-ring–opened 7′-carba-4BD–bound D14 (green) and GR24-bound D14 (PDB code 5DJ5) (blue) in three different orientations. The bound D-ring–opened 7′-carba-4BD molecule and GR24 are presented in orange and yellow, respectively. The r.m.s.d. for the Cα atoms was 0.38 Å.

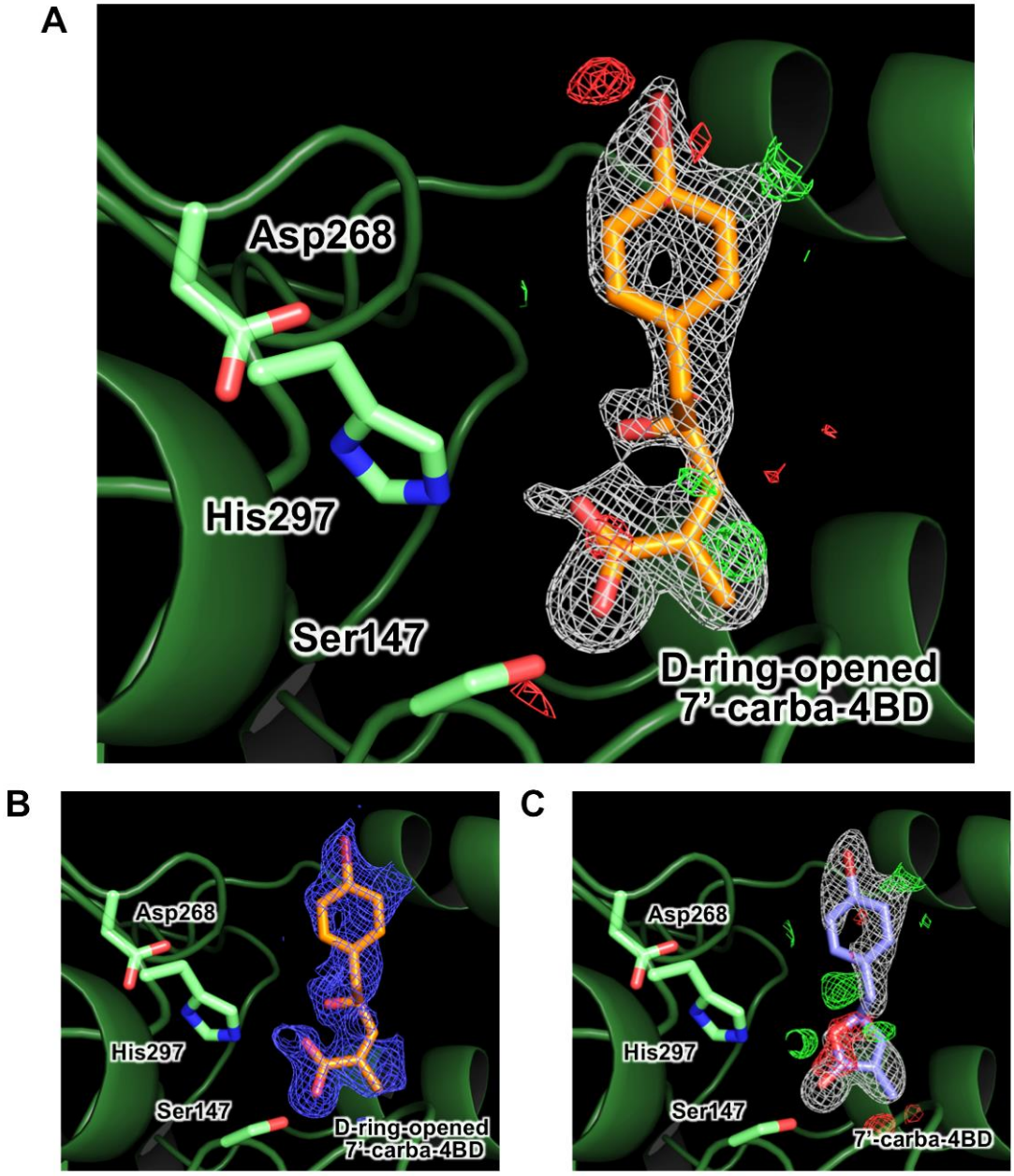

Fig. S8 Validation of the electron density map derived from D-ring-opened 7′-carba-4BD observed in the pocket. The residues forming the catalytic triad (green) and D-ring-opened 7′-carba-4BD (orange) and 7′-carba-4BD (purple) are shown as a stick model. The $2F_o-F_c$ maps were colored white and contoured at 1.0 σ. This represents the predicted model, whereas the F_o-F_c maps are colored green (3.0 σ) and red (−3.0 σ). The green mesh indicates where atoms are missing in the current model, while the red mesh indicates where atoms are present in the model but not in the crystal. The blue mesh indicates the F_o-F_c omit map contoured at 3.0 σ. (A) The maps were calculated using submitted coordinates to PDB (accession code 5YZ7) in this study. They indicate a reasonable fit to the D-ring-opened 7′-carba-4BD complex, and almost no peaks were found in the F_o-F_c maps. (B) Omit maps were calculated after excluding D-ring-opened 7′-carba-4BD. A positive density that was well-fitting to D-ring-opened 7′-carba-4BD was detected in the pocket. (C) The maps were calculated after replacing the D-ring-opened 7′-carba-4BD with 7′-carba-4BD, followed by refinement. Note that the red mesh was observed in the closed D-ring, indicating that these modelled atoms are not present in the crystal.

Supplementary Fig. S9 NMR Spectrums of (±)-1′-carba-GR24 (enantiomers of 3a and 3c)

^{1}H NMR spectrum

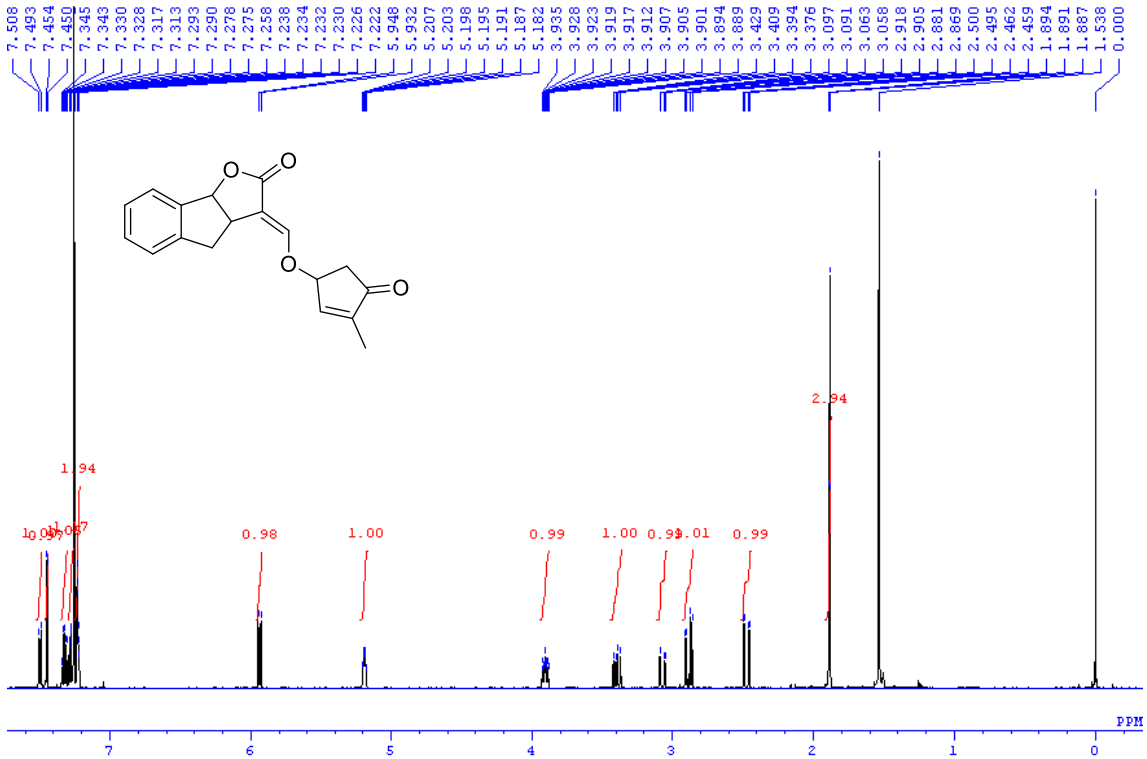

^{13}C NMR spectrum

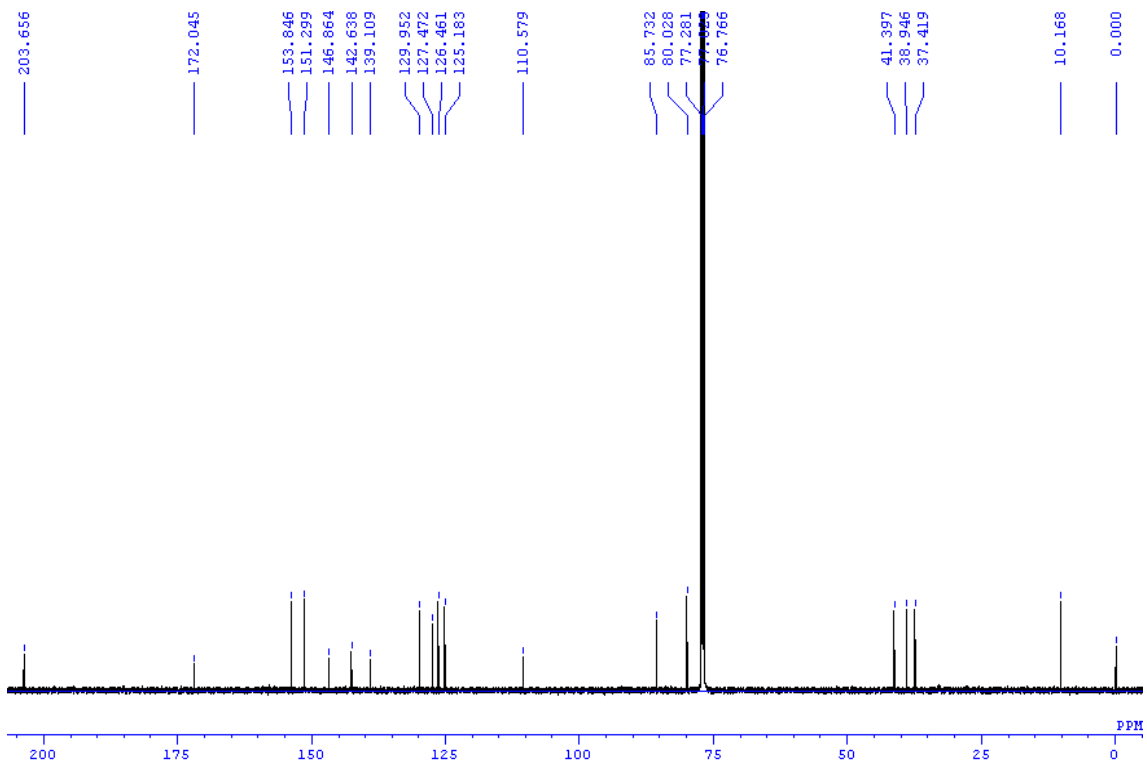

Supplementary Fig. S10. NMR Spectrums of (±)-1′-carba-GR24 (enantiomers of 3b and 3d)

^{1}H NMR spectrum

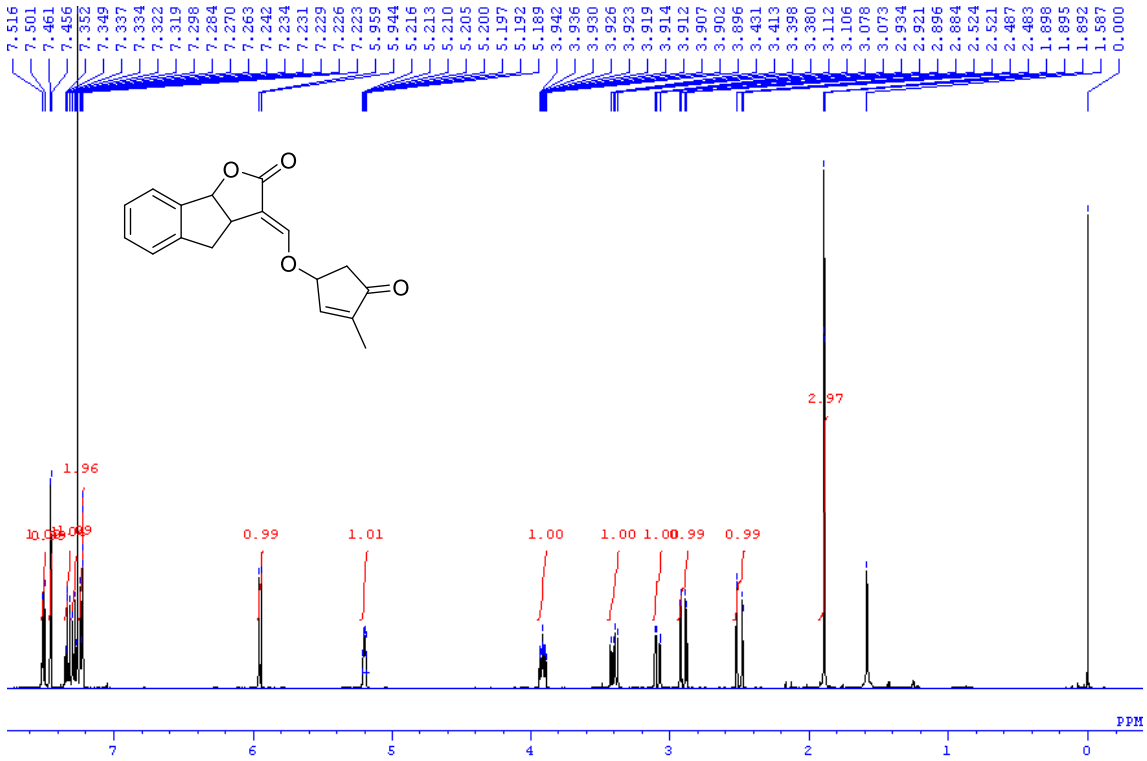

^{13}C NMR spectrum

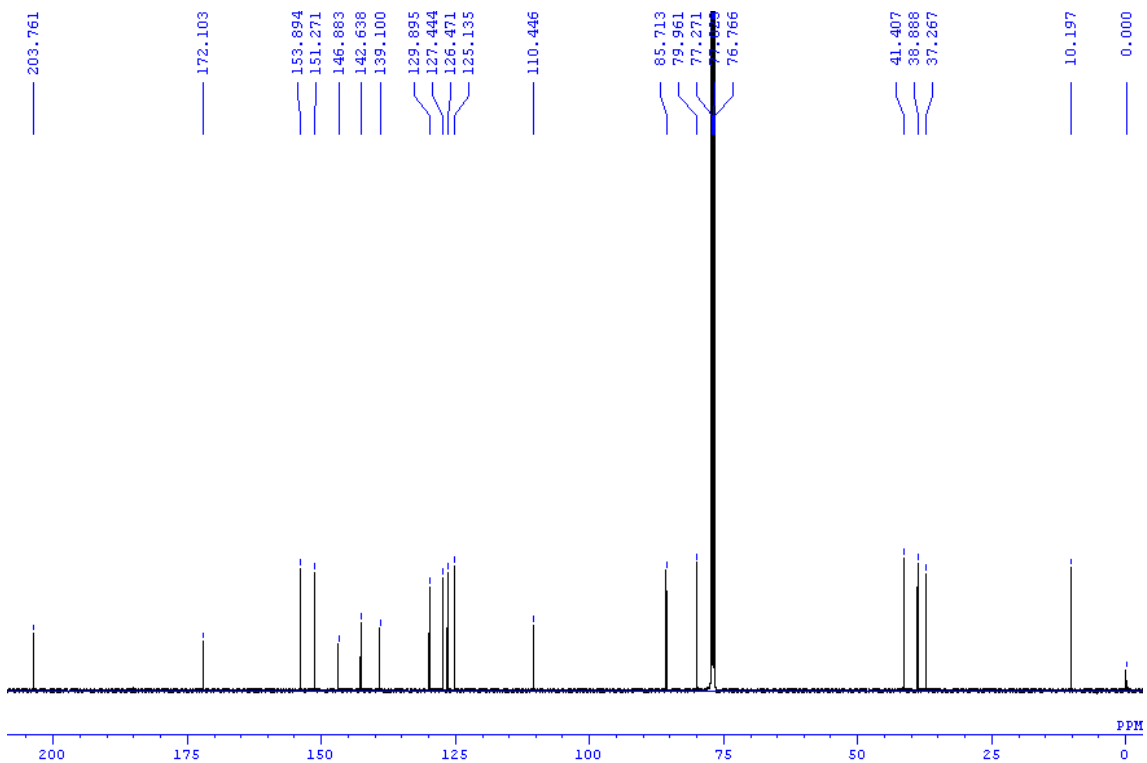

Supplementary Fig. S11. NMR Spectrums of (±)-1′-carba-4BD (compound 4)

^{1}H NMR spectrum

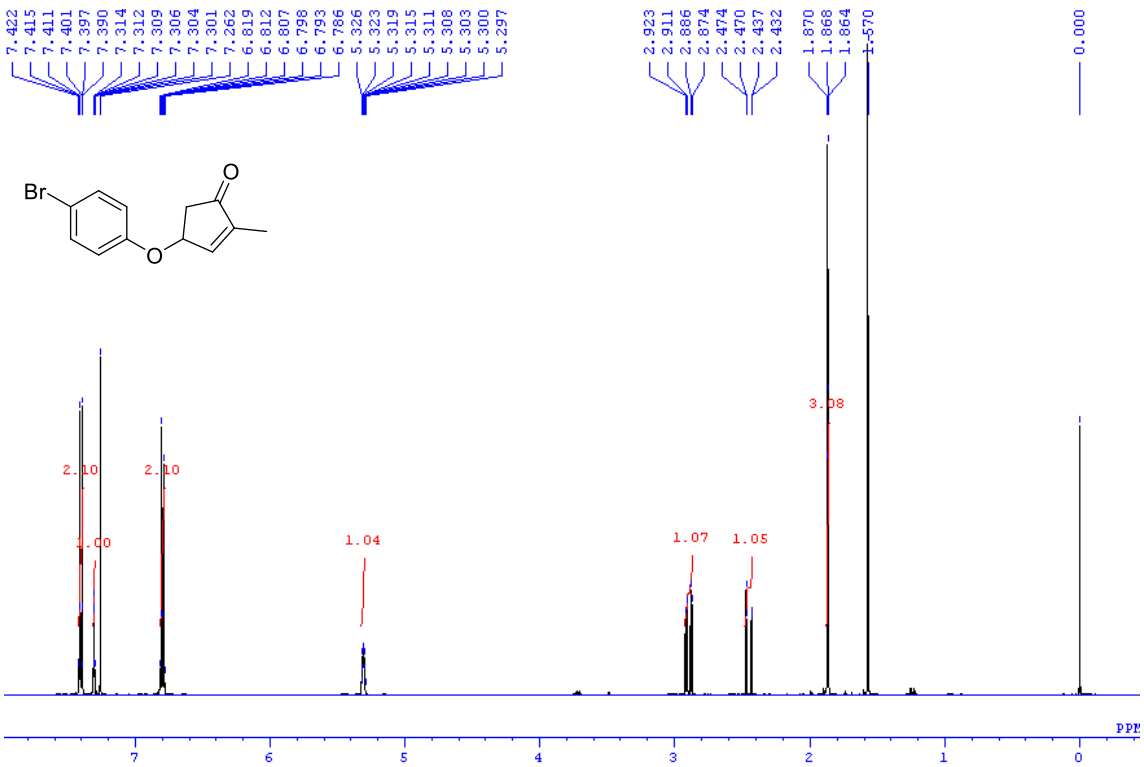

^{13}C NMR spectrum

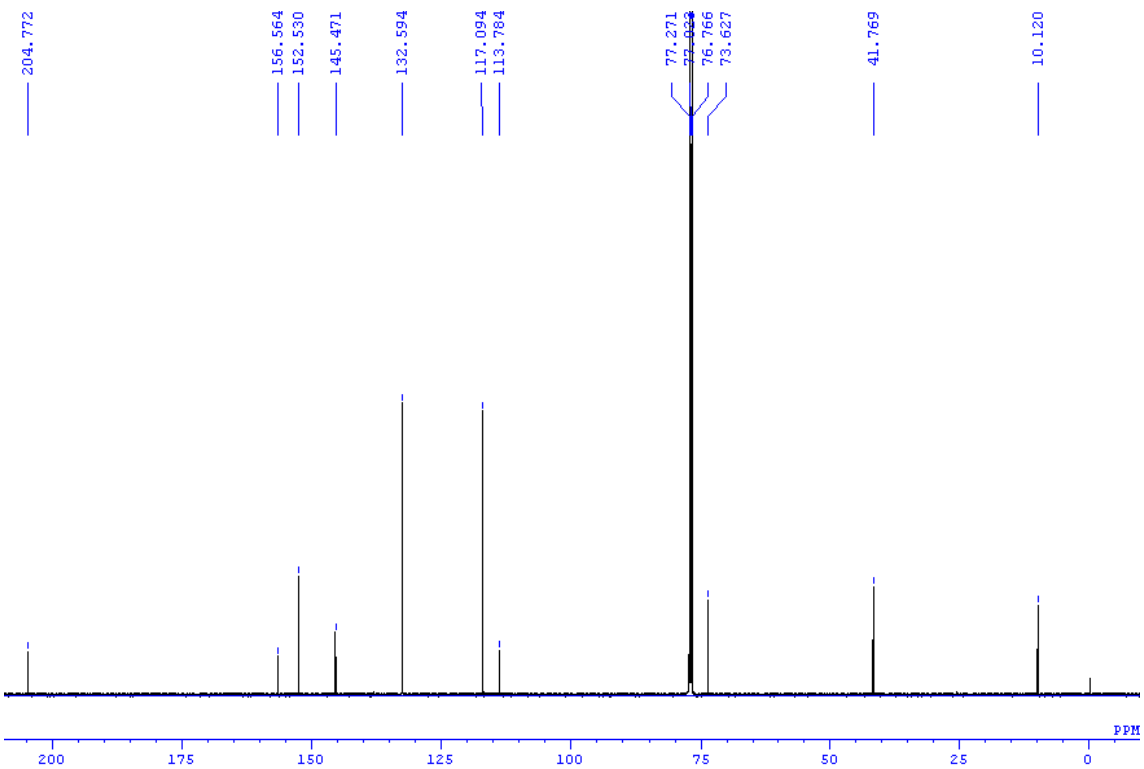

Supplementary Fig. S12. NMR Spectrums of (±)-7′-carba-4BD (compound 5)

^{1}H NMR spectrum

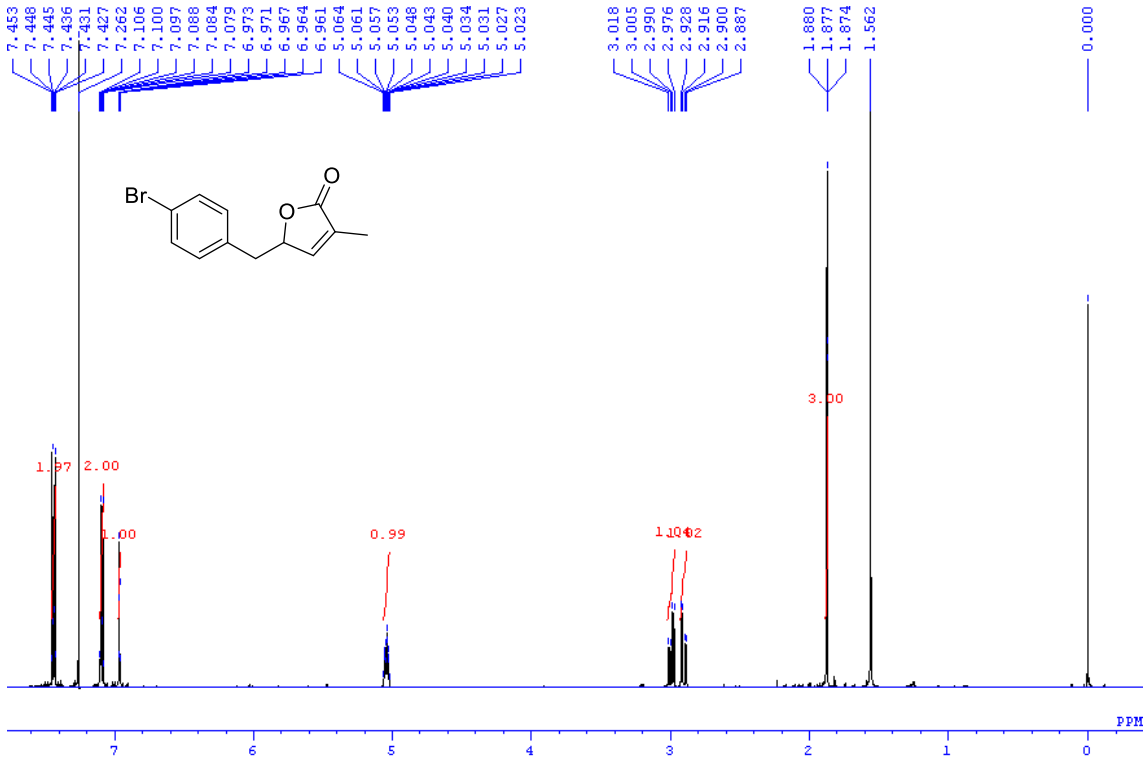

^{13}C NMR spectrum

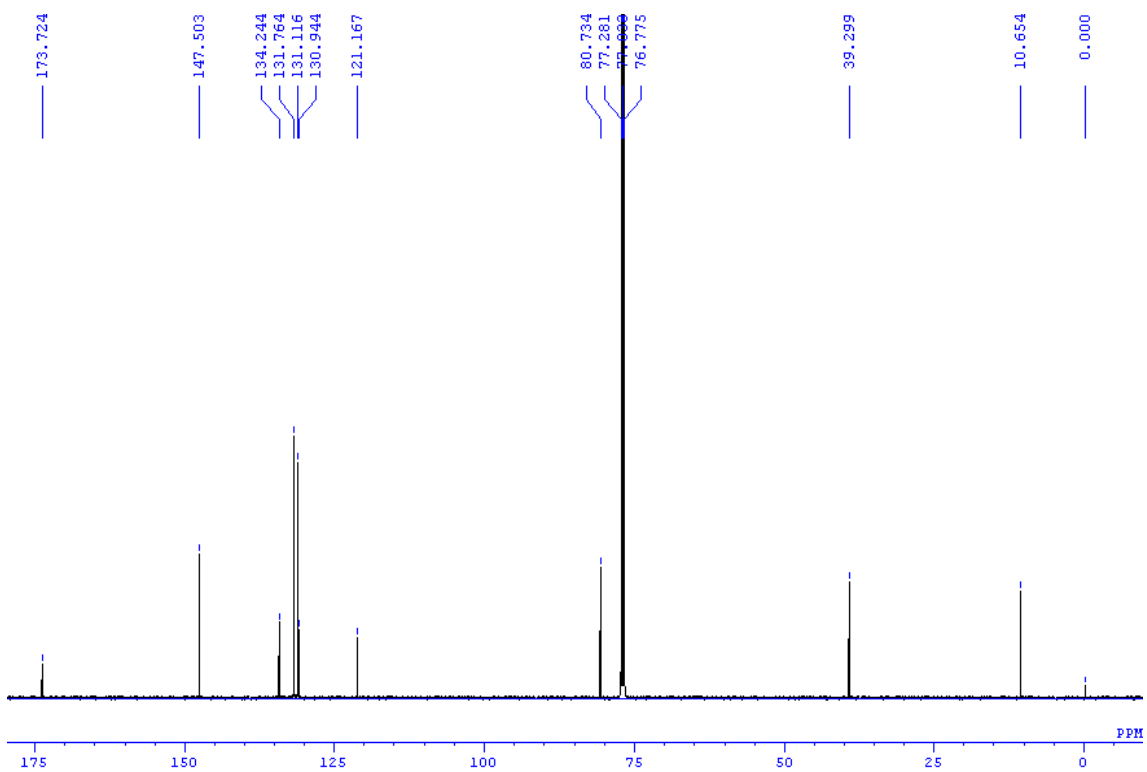

Table S1. X-ray data collection and refinement statistics

	D14–D-ring-opened 7'-carba-4BD complex (5YZ7)
Data collection	
Space group	$P2_12_12_1$
Cell dimensions	
a, b, c (Å)	48.50, 88.80, 118.60
α, β, γ (°)	90, 90, 90
Resolution (Å)	1.90 (2.01 - 1.90)
No. of observations	556,557
No. of unique reflections	40,129
R_{merge}[a] (%)	5.4 (23.8)
$I/\sigma I$	38.8 (12.2)
$CC_{1/2}$[b] (%)	100.0 (98.5)
Completeness (%)	97.1 (89.4)
Redundancy	13.9 (13.2)
Refinement	
Resolution (Å)	37.54 - 1.90
No. of used reflections	76,731
R_{work}[c] / R_{free}[d] (%)	18.9/22.7
No. of atoms	
Protein	4,102
Ligand	32
Water	435
B factors (Å^2)	
Protein	19.7
Ligand	43.3
Water	25.8
r.m.s. deviations	
Bond lengths (Å)	0.005
Bond angles (°)	0.862
Ramachandran plot (%)	
Favored	97.9
Allowed	2.1
Outliers	0.0

Values in parentheses correspond to the highest-resolution shell.

[a] $R_{merge} = \sum_{hkl}\sum_i|I_i(hkl)-\langle I(hkl)\rangle|/\sum_{hkl}\sum_i I_i(hkl)$.

[b] $CC_{1/2}$ is the percentage of correlation between intensities from random half-datasets.

[c] $R_{work} = \sum_{hkl}||F_o(hkl)|-|F_c(hkl)||/\sum_{hkl}|F_o(hkl)|$.

[d] R_{free} is the R_{work} calculated for 5% of the data set not included in refinements.